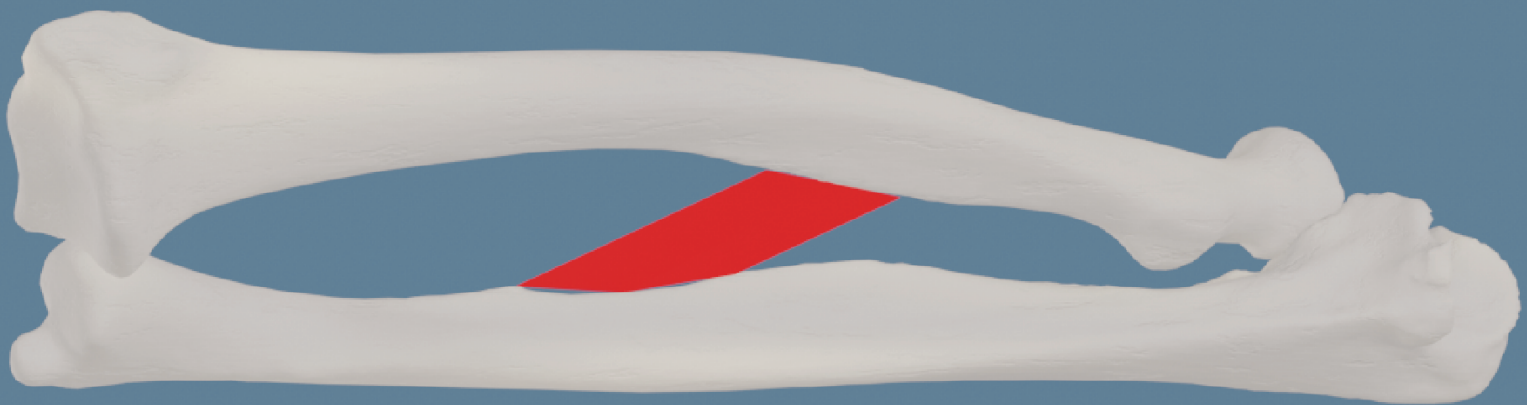


Forearm Rotation after Malunited Diaphyseal Fracture: Predicting Range of Motion with a Kinematic Model

Master Thesis
Technical Medicine
Derek van Loon



Explaining Rotational Restriction after Diaphyseal Forearm Fractures by Modeling Pronation and Supination movement

by

Derek van Loon

Student number: 4387295
Project duration: March, 2021 – February, 2022
Thesis committee: Dr. Joost Colaris Erasmus Medical Center, supervisor
 Prof. Dr. DirkJan Veeger Technical University Delft
 Drs. Eline van Es Erasmus Medical Center

An electronic version of this thesis is available at <http://repository.tudelft.nl/>.

Abstract

Introduction Fractures of the diaphysis of the radius and/or ulna are most common in children from 5 to 14 years old and take up to 40% of all pediatric fractures. Patients with a diaphyseal fracture of the forearm can develop a malunion: healing of the bones in non-anatomical position. This can lead to pain, cosmetic differences and a limitation of pronation and/or supination. A malunion with an angulation of at least 15 degrees leads to a limitation in rotation of the forearm in 60% of the cases. However, it is not known how a malunion leads to a rotational limitation and why certain patients have a predominant supination limitation and some have a predominant pronation limitation. It is hypothesized that the distance between the bones can explain the limitation: a too small distance leads to bone impingement and blocking the rotation, a too large distance leads to contracture of the central band, a ligament between the radius and ulna.

Aim The aim of this research is to explain the loss of rotational function in malunited forearms by using a kinematic model in which bone impingement and contracture of the central band can be recognized.

Method Fifteen (n=15) patients were included who developed a malunion after a one-sided, both-bone diaphyseal fracture of the forearm during childhood (age < 18) which led to a range of pronation and/or supination lower than 50 degrees. Their range of motion was measured and CT-scans were made of both forearms, from which three-dimensional bone surface models were retrieved. A kinematic model for pronation and supination of the forearm was developed in which the patient specific anatomy was used to detect bone impingement, measure central band length (CBL) and measure minimal interosseous distance (MID) between the radius and ulna. Bone impingement and CBL were used for prediction of the range of motion of the malunited forearms, MID was used to compare the distance between the bones at maximum supination and pronation between the affected and unaffected forearms of the patients. Central band length relative to the neutral position was calculated in unaffected forearms to define a threshold for contracture. Bone impingement was defined as overlapping of the bone surface models. The root mean squared error (RMSE) between in vivo measured range of pronation, supination and full range and the predicted values is calculated.

Results All fifteen patients showed bone impingement as reason for limiting pronation, fourteen patients showed contracture of the central band as reason for limiting supination. By setting the threshold at 103% of the relative central band length, the pronation, supination and full range of thirteen patients could be predicted with a RMSE between 15.5 and 17.9 degrees. Bone distance was significantly lower in malunited forearms than in unaffected forearms in maximum pronation. In supination this effect was much less clear. The kinematic model showed an error less than one millimeter and one degree for translation and rotation compared to cadaveric scans in different pronation and supination positions.

Conclusion The kinematic model showed that bone impingement and central band contracture are the best explanations for limiting pronation and supination of malunited forearms. Prediction is difficult because the kinematic model uses the neutral position as starting point, which is not always clear because the kinematics of forearm rotation still has some unknowns and the central band origin and insertion is now located based on a cadaveric study.

Contents

1	Introduction	1
1.1	Background	1
1.1.1	Pronation and supination of the forearm	1
1.1.2	Bone anatomy of the forearm	1
1.1.3	The proximal and distal radio-ulnar joints	2
1.1.4	The interosseous membrane of the forearm	2
1.1.5	Rotational limitation	2
1.1.6	Measuring malunion	4
1.1.7	Three dimensional bone models	4
1.1.8	Forearm rotation after malunited diaphyseal fracture	4
1.1.9	Modeling forearm rotation	5
1.2	Aim and objectives	5
2	Relation between bone deformation and rotational restriction	7
2.1	Introduction	7
2.2	Method	7
2.2.1	Patient selection	7
2.2.2	From bone surface models to deformation measurements	7
2.2.3	Grouping patients	10
2.2.4	Statistical calculations	10
2.3	Results	10
2.4	Discussion	10
3	Kinematic model of pronation and supination of the forearm	15
3.1	Introduction	15
3.2	Method	15
3.2.1	General working principle of the rotation	15
3.2.2	Proximal radio-ulnar joint	16
3.2.3	Distal radio-ulnar joint	16
3.2.4	Validation	16
3.3	Results	19
3.4	Discussion	20
4	Bone distance during pronation and supination as measured from a kinematic model	21
4.1	Introduction	21
4.2	Method	22
4.2.1	Determining the neutral position	22
4.2.2	Bone impingement	22
4.2.3	Central band length	22
4.2.4	Minimum interosseous distance	23
4.2.5	Statistical tests	23
4.2.6	Predicting range of motion of unaffected forearms	23
4.3	Results	24
4.3.1	Minimum interosseous distance and bone impingement	24
4.3.2	Central band length	27
4.3.3	Prediction of range of motion in affected forearms	27
4.4	Discussion	27

5	Clinical relevance and future research	31
A	Individual patient data	33
B	Validation data	35
C	Distance graphs	37

Introduction

1.1. Background

In the introduction basic medical and technical knowledge is briefly explained. First, function and normal anatomy of the forearm is explained. Then is explained what happens for a patient with a diaphyseal fracture of the radius and ulna. The technical principles to understand the pipeline from patient to 3D rotational bone models are briefly addressed. Then the research question is presented.

1.1.1. Pronation and supination of the forearm

Pronation and supination are terms to describe the position of the hand palm relative to the body. When the arms are positioned along the sides of the body, if the hand palm is pointing forwards and the thumb is pointing away from the body, this is called supination. Pronation is when the hand palm is pointing backwards and the thumb is pointing to the body. The neutral position is when the palm is pointing inwards to the body and the thumb points forwards. This must not be confused with the anatomical position, which is defined as the palms pointing forwards, thus in supination.

The range of pronation and supination is measured from the hand in neutral position and the elbow in 90 degrees flexion. While holding the elbow fixated to the side of the body, the forearm is rotated to maximum supination or pronation and measured with a goniometer. [11] Normal ROM are respectively 70 to 100 degrees supination, 60 to 80 degrees pronation and thus a full arc of 130 to 180 degrees [48]. In daily life, a range of motion of 50 degrees of pronation and 50 degrees of supination is considered sufficient [58]. However, some more contemporary tasks like typing require a larger range of pronation.

1.1.2. Bone anatomy of the forearm

The forearm consists of two longitudinal bones: the radius and the ulna. In the anatomical position the radius is on the lateral side and the ulna on the medial side of the body. The two bones articulate at two joints: the proximal radio-ulnar joint (PRUJ) and the distal radio-ulnar joint (DRUJ) [62]. During rotation of the wrist the distal radius rotates around the ulnar head distally, while proximally the radius head rotates in the radial notch of the ulna. This creates a diagonal rotation axis from the proximal radial head to the distal ulnar head [53], see figure 1.1. From supination to pronation, the radius extends over the ulna and rotates the wrist. To make pronation possible, the radius and ulna are curved in such a way that there is room for the radius to lay over the ulna. [51]

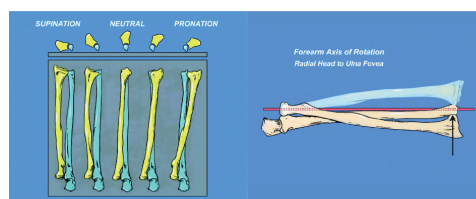


Figure 1.1: Left: visualized forearm rotation [29]; Right: axis of rotation [29]

1.1.3. The proximal and distal radio-ulnar joints

In the PRUJ the head of the radius rotates in the radial notch of the ulna. The radius is kept in place by two ligaments. The quadratum ligament connects the radial notch of the ulna to the neck of the radius. While providing stability during rotation, it also limits supination by 10 to 20 degrees and pronation by 5 to 8 degrees [56]. Secondly, there is the annular ligament which is connected to the anterior and posterior border of the radial notch of the ulna and surrounds the radial neck and head. The annular ligament stabilizes the movement of the radial head during rotation. For as far as is known, it does not limit pronation and supination [17].

Distally, the radius and ulna are connected by the distal radio-ulnar ligament, which consists of four parts. There are two dorsal ligaments and two palmar ligaments, both have one deep ligament and one superficial ligament [20]. The palmar and dorsal ligaments extend from the sigmoid notch of the distal radius. The superficial parts converge into the base of the ulnar styloid, while the deep parts attach to the fovea of the ulnar head. In maximum supination the palmar radio-ulnar ligaments (PRUL) control the movement of the radius, while in maximum pronation this is controlled by the dorsal radio-ulnar ligaments (DRUL) [29]. These ligaments are the primary stabilizers of the DRUJ, so are important in the rotation and movement of the radius. These ligaments do not have a known, limiting effect on the rotational movement.

1.1.4. The interosseous membrane of the forearm

While the radius and ulna are only in direct contact within the joints at the distal and proximal side, between their diaphyses the interosseous membrane (IOM) is located. This membrane creates a fibrous joint called a syndesmosis. Because of its strong collagen fibers, it provides longitudinal stability, prevents separation and ensures weight distribution along the forearm. [5]

Within the membrane multiple ligaments and bundles of ligaments are located, which provide the most stability. [41] The IOM can be divided into the proximal, middle and distal portion. Of these three, the middle portion contains the most important ligament: the central band (CB) and some additional accessory bands (AB). The proximal portion contains the proximal oblique cord (POC) and dorsal oblique cord (DOC), while the distal portion only contains the distal oblique bundle (DOB). The variation in presence and location of the oblique ligaments is large and they only improve stability when present, but do not contribute to joint instability when cut. [28, 55]

The CB is the most broad and thick ligament of the IOM and provides the most stability of the ligaments in the IOM. [26] It originates on the radius and inserts on the ulna. The fibers are oriented diagonally: the insertion on the ulna lies more distally than the origin on the radius [41]. Furthermore, the fibers spread out, so that the insertion is broader than the origin. The strain of the CB is the highest of all the ligaments, which in vivo lead to an almost fixed length during pronation and supination and ensures the most stability. [3] The ABs are variable in amount, length and thickness as well, but when present they span in the same direction as the CB and mostly support the CB. [41] In research, the term 'central band' is therefore sometimes used for the collection of the CB and additional ABs. More recent research however points out that because of the variability in presence of ABs, these only improve the stability of the CB, just as the proximal and distal ligaments in the IOM. It can be concluded that the CB is therefore the most influential ligament of the IOM.

1.1.5. Rotational limitation

One of the reasons for a rotational limitation of the forearm is a diaphyseal fracture. Fractures of the diaphysis of the radius and/or ulna are most common in children from 5 to 14 years old and take up to 40% of all pediatric fractures. [23, 50] Gold standard in treatment is closed reduction and casting, which leads to adequate alignment in 70% to 90% of the cases. [54] However, the amount of angulation, displacement and location of the fracture as well as the age of the patient must be considered in order to determine whether open reduction is needed. [60] In case of a malunion of the bone, the patient can show symptoms, such as pain, stiffness, loss of pronation and supination, a painful DRUJ, and aesthetic problems [40].

If surgery is needed is at the moment decided based on the angulation of the radius and ulna. 10 degrees of angulation can be accepted: a larger malunion is often considered for surgery [54]. However, if the patient is 9 years or younger, 15 degrees of angulation is still acceptable because the bones still remodel during growth [16]. In case of severe malalignment, surgery can be done using plates or an intramedullary nail [54].

In case of a rotational restriction functional loss is calculated by comparing the ROM of the affected and unaffected arm of the patient because of the large spread in normal range of motion between individuals. [48] If the range of pronation or supination is below 50 degrees, this is considered as a clinically relevant loss [58]. Due to the lower rotational ROM, the shoulder joint is used to compensate [43]. These compensatory

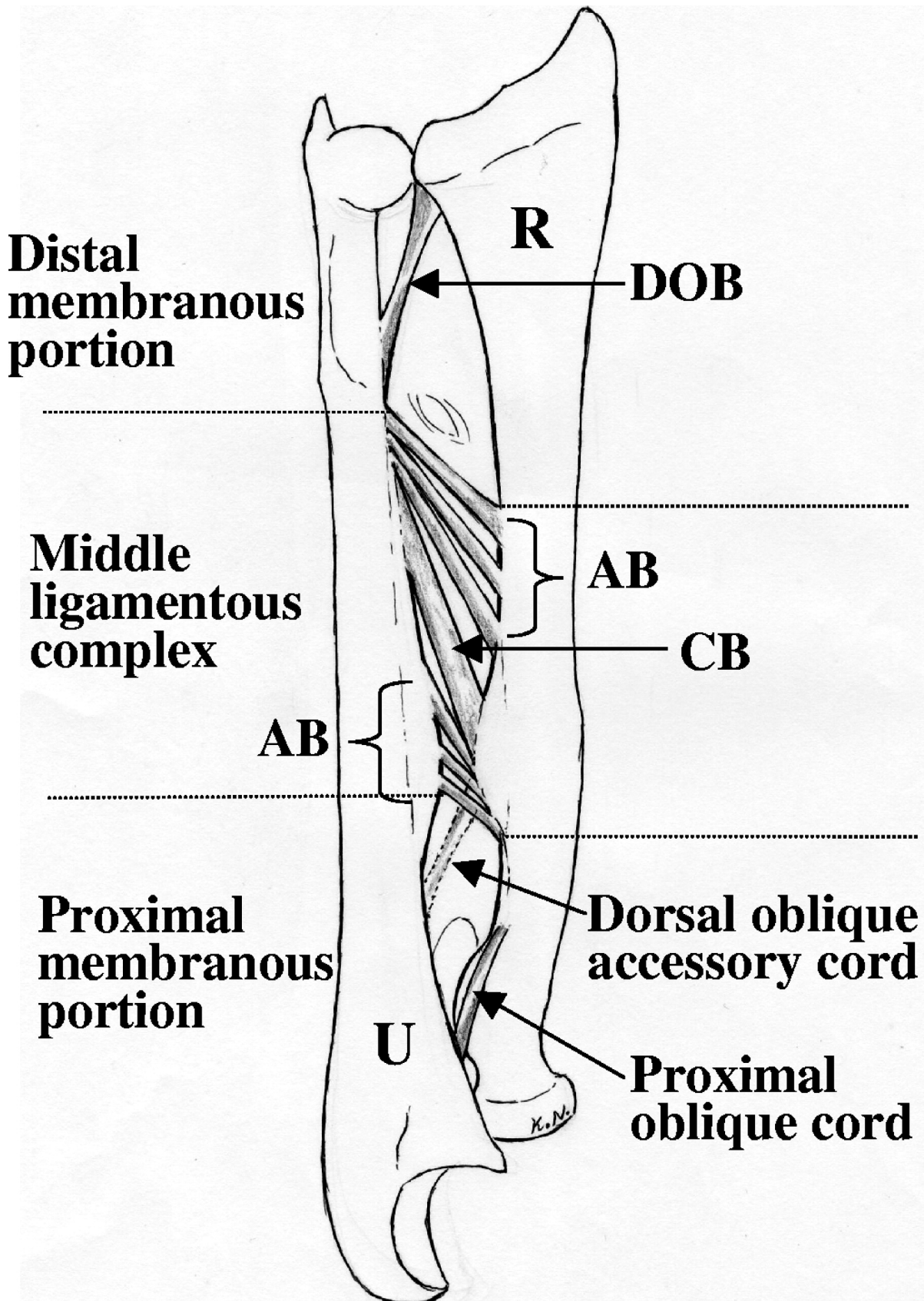


Figure 1.2: Ligaments of the interosseous membrane [41]

movements could be prone to other risk of injuries, especially in patients with long lasting limitations.

1.1.6. Measuring malunion

A malunion is defined as a fractured bone which is healed in an abnormal position. Malunions are measured as an angular deformity of a bone in comparison to the unaffected, contralateral bone. This cannot be measured during physical examination, so x-rays images are made on which the angulation of the bones can be measured and compared. An angulation can extent itself in three different directions: dorsovolar angulation (DVA), also known as extension-flexion deformity, measured in the sagittal plane, radioulnar angulation (RUA), also known as varus-valgus deformity, in the coronal plane, and internal angulation (IA), also known as pronation-supination deformity, in the axial plane. DVA can be measured in the lateral view and RUA in the AP view of x-ray images. IA is not directly measurable in x-ray images, but an estimation can be made based by looking at the visibility of bone landmarks in certain views [13].

More recently, the introduction of computed tomography (CT) made measuring deformity easier and more precise, especially the internal angulation [44]. The same method as on x-ray images can be used, so manually measuring the angle between points with the advantage of an image with a higher resolution and in three-dimensions. The other method is to retrieve three dimensional bone surface models from these scans, but more on that later. This three dimensional representation of the bone makes the comparison between affected and unaffected bone easier because the models can be aligned on the proximal parts, which then immediately shows the deformity. After placing bone landmarks indicating the anatomical planes, the angulation can be measured. It is also the easiest way to understand the patient specific anatomy: it is almost a one-on-one representation.

1.1.7. Three dimensional bone models

Three dimensional bone models are a digital representation of the shape of a bone. The pipeline from patient to three dimensional bone model consists of several steps. These will be explained in the process of retrieving the models from the malunited forearm and the contralateral, unaffected forearm of a patient.

First, a CT scan is made of both forearms of the patient. Both arms must be scanned in the neutral position. To do this, the patient lies in prone position with their arms stretched out above their heads with the palms facing each other. The CT-scan generates a series of axial x-ray images from the elbow to the hand. In these images the bone is colored white and surrounding soft tissue gray. Stacking these images leads to a three dimensional image of the forearm. Because each layer has a certain thickness, the pixels are essentially not flat but a small volume. Therefore, they are called voxels: pixels with a volume, comparable with cubes.

In every axial image the radius and ulna are segmented. The voxels in every layer representing the bones are selected which can be done manually or using a semi-automated or fully-automated method. The selected voxels are then connected between the layers. Stacking the segmented voxels of each layer creates a three dimensional object consisting of all those voxels in the shape of the bone. Then an algorithm is used to generate a mesh from the object. A mesh is a representation of the surface of the volume and consists of points, vertices, connected by edges which form faces in the form of triangles.

From a CT scan the radius and ulna are segmented. The voxels representing the bones form a volume of which the surface can then be represented by triangulation: a collection of points, also known as vertices, connected by edges, forming triangular faces. Multiple faces forming a three dimensional surface is called a polygonal mesh. This mesh is a patient specific model, which is easier to interpret than the original CT-scan and it can be used for multiple purposes in modern healthcare, such as surgical planning, augmented reality and 3D printing.

1.1.8. Forearm rotation after malunited diaphyseal fracture

It has been proven that restoring original anatomy with an osteotomy can restore rotational function of a malunited forearm [47]. The unaffected forearm is used as reference as how the original bones were shaped [47]. With a CT-scan of both forearms in neutral position, 3D bone models of the radius and ulna of the affected and unaffected forearm can be made using segmentation. The unaffected forearm bones are then mirrored and aligned with the affected bones to analyze the deformity and plan the intervention to reshape the bones.

While the relation between diaphyseal malunion of the radius and/or ulna and a rotational limitation seems obvious at first, the clinical presentation of patients with a malunion is not unambiguous. Multiple papers describe the link between limitation and malfunction, but only bone deformity is not enough to explain why and how a limitation occurs. Only 60% of the children with an angulation of 16 degrees or more

after a single-bone fracture compared to the unaffected forearm have a clinical significant limitation. [12] So, while the chance of a rotational limitation increases with a larger angulation, the limitation can not only be explained from the degree and direction of single-bone angulation.

1.1.9. Modeling forearm rotation

Recent research points out that the distance between the bones is altered, which leads to a limitation of rotational function [1]. In short, deformation of the radius or ulna can have two effects on the distance between the radius and ulna: (1) the deformation of one bone is directed towards the other and bone impingement occurs, or (2) the deformation is directed away from the other bone and contracture of the interosseous membrane, especially the CB, occurs.

To analyze and measure these effects the full arm must be visualized during the full rotational movement. While this is possible with four-dimensional computed tomography (4DCT), this technique has a low resolution for a large field of view (FOV), what is needed to scan the full forearm. Furthermore, the radiation dose of a 4DCT-scan of only the wrist is about three times higher than a static CT-scan, without any known benefit at the moment. [22, 9] Also, most soft tissue is not clearly visible on a CT-scan, so magnetic resonance (MR) images are preferred. Nevertheless, dynamic MR scans have an even lower resolution than a 4DCT-scan and dynamic soft tissue imaging is not clinically feasible at the moment. Visualizing the CB dynamically is therefore very difficult.

A kinematic rotational model of the forearm could provide a solution. Static visualization of bones is possible and three dimensional bone surface models can be retrieved from these scans. From a CT scan in neutral position, 3D models of the radius and ulna can be retrieved. Using the bone shapes of the PRUJ and DRUJ the movement can be simulated by calculating a rotation axis from the proximal radial head to the distal ulnar head. In this way, bone to bone distance can be visualized and measured during a mimicked rotation. By comparing these measurements with the ROM of unaffected forearms, it can be learned if rotational restrictions after a diaphyseal malunion can be explained by the combination of bone impingement and central band contracture.

1.2. Aim and objectives

The aim of this research is to explain the loss of rotational function in malunited forearms by using a kinematic model in which bone impingement and contracture of the central band can be recognized. First, to answer this question, the deformity of the radius and ulna of this research population will be linked to rotational restriction: the standard for reporting malunions. Second, a kinematic model for the rotation of the radius during forearm rotation will be developed and validated using scans of unaffected, cadaveric forearms. Third, the kinematic model will be used on unaffected and affected forearms to measure bone impingement, central band length and minimal interosseous distance and link this to the patients' range of pronation and supination. Bone impingement and central band length will be used to predict the range of motion in malunited forearms.

2

Relation between bone deformation and rotational restriction

2.1. Introduction

Fractures of the diaphysis of the radius and/or ulna take up to 40% of all pediatric fractures [50]. Gold standard treatment is closed reduction and casting, which leads to adequate alignment in 70% to 90% of the cases [54]. When repositioning is not done correctly, a malunion can occur, which might lead to a limited range of pronation and/or supination of the forearm [12]. While the chance on a rotational limitation rises with a larger deformity, there is no cut-off value for deformity and limitation. This could be because the angulation is measured on x-ray images. This imaging technique is limited because it only shows a projection, not a full three dimensional view. For distal radius malunions it is shown that measurements on x-ray can differ from measurements done on computed tomography (CT) scans, especially when angulation is large, more than 21 degrees [33]. Measuring internal angulation is the most difficult on x-ray and CT provides a helpful solution [44]. This research uses an automatic method to calculate deformity of the malunited radius and ulna of fifteen patients with a rotational restriction of the forearm after a both-bone fracture. Aim is to relate degree of deformity of the radius and ulna to the loss of rotational function of patients. This is done by correlating loss of function compared to the contralateral side and directional angulation, and by comparing groups of patients based on their directional angulation and prominent directional loss.

2.2. Method

2.2.1. Patient selection

The patients in this study were included in the 3DOOM study of the Department of Orthopedics and Sports Medicine of Erasmus Medical Center in Rotterdam. All included patients (n=15) had a forearm malunion after a diaphyseal both-bone fracture sustained during childhood. Malunion was defined as a healed bone in an abnormal, non-anatomical position when compared to the unaffected side of the patient as measured on x-ray images. The diaphysis was defined as the part of the bone between 20% and 80% of its length [40]. CT-scans of both forearms had to be available. Range of motion of the affected and unaffected forearm were measured in these patients. Loss of function is calculated compared to unaffected side. The range of pronation and/or supination of the affected forearm had to be lower than 50 degrees.

2.2.2. From bone surface models to deformation measurements

From the creation of bone surface models to deformity measurements, the following steps were taken: mesh filtering, coordinate system definition, surface registration, obtaining angulation. This pipeline is based on the deformity measurements from Miyake et al. [34]. All steps will be explained below. All code was written in Python 3.8.11 [59]. For mesh filtering the Python library of MeshLab was used, version 2021.7. [39]. For mesh and point cloud calculations the library of Trimesh was used, version 3.9.31. [14].

Mesh Filtering The patient underwent a CT scan (slice thickness 0.7 mm) in preparation for a corrective osteotomy. Both arms were scanned in one scan. The patient was laying in prone position with their sholders in maximal abduction, elbows in maximal extension, hand palms facing each other. From this scan the radii

and ulnae were segmented semi-automatically using software called Mimics [31]. The segmentations were then converted to three dimensional surface models using the same software. These surface models had between 5000 and 10000 vertices, dependent on size of the bone, with most points in the proximal and distal surfaces of the bones. To increase the number of vertices along the diaphyses to make point cloud registration possible, the meshes underwent subdivision filtering. The target amount of surfaces was 15000 and a range of $\pm 5\%$ was allowed.

Coordinate system definition To measure difference in shape between two bones, the unaffected bone must be placed in a coordinate system. The coordinate system used in this research is based on the standard of the International Society of Biomechanics (ISB) [63]. This was done by recognizing bone landmarks on the surface models, which are visualized in figure 2.1. The bone was placed into the coordinate system based on these landmarks to standardize planes and directions. For the radius the bone landmarks placed on the z-axis were the center of the depression on the proximal head and the center of the ridge between the radioscaphoid fossa and the radiolunate fossa. The y-axis projected from the radial styloid and the center of the ridge between the fossae on the distal radius and is perpendicular to the z-axis. The x-axis is then automatically the perpendicular to the x and z-axis.

Following the same guideline, the coordinate system of the ulna would be based on its relative position to the radius. Because this does not work for measuring deformity, some points in addition to those of the ISB standard were placed. The ulnar landmarks defining the z-axis were the center of the coronoid process and the center of the ulnar dome. The y-axis is perpendicular to the z-axis and is projected from the ulnar styloid towards the center of the ulnar dome. The x and y axis are different between the radius and ulna because the anatomical coordinate system is defined in 90 degrees of supination. The x-axis is perpendicular to the y and z-axis. The landmarks are visualized in figure 2.2.

Surface registration After placing landmarks, the unaffected bone was mirrored to be comparable with the deformed contralateral bone. This is in case of the radius and ulna reflection of the sagittal plane. The affected bone is superimposed on the unaffected bone. The affected bone must overlap the unaffected bone proximally. To reach this position the proximal 20% of the affected bone was registered on the 20% of the proximal length of the unaffected bone. This is done with a iterative closest point (ICP) algorithm. Because the initial position of the affected bone is of importance to the outcome of this algorithm, the initial position is standardized using a procrustes registration. This optimizes the alignment of a selection of points, in this case three bone landmarks in the proximal part of the bone. For the radius these are the center of the fovea, the radial tuberosity and the centroid of the cross-section of the bone at 20% of its length. For the ulna these are the center of the coronoid process, the tip of the coronoid process and the centroid of the cross-section of the bone at 20% of its length.

Then, the distal 20% of the unaffected bone is registered on to the 20% of the affected bone as target. The registrations consisted of two steps: first a procrustes registration was done, followed by an iterative closest point (ICP) registration. For the proximal procrustes registration, the landmarks of the radial fovea, radial tuberosity and the centroid of the cross-section at 20% of the length of the bone were used. For the distal procrustes registration the radial styloid, center of the ridge and the centroid of the cross-section at 80% of the length were used.

Obtaining angulation Without a deformity present, the affected and unaffected bones will almost fully overlap when they are proximally aligned apart from small differences between sides. In the case of a deformed bone, the deformity is visible because the distal part of the affected bone is not overlapping. From the situation in which the affected bone is aligned with the unaffected bone based on the proximal registration, the transformation needed to align the unaffected bone with the affected bone with the distal 20% is considered the deformity of the affected bone, see figure C.31. The transformation matrix describing the movement of the unaffected bone from proximal alignment to distal alignment is considered the deformity. The transformation matrix can be converted to Euler angles in the x, y and z-direction. These angles describe the deformity in the coronal, sagittal and axial plane respectively.

Rotation around the x-axis corresponds with radial (+) and ulnar (-) deformity, thus describing radioulnar angulation (RUA), rotation around the y-axis corresponds with dorsal (+) and volar (-) deformity, thus describing dorsovolar angulation (DVA), rotation around the z-axis corresponds with pronation (+) and supination (-) angulation, thus describing internal angulation (IA).

In addition to these three angulations, the total angulation (TA) is calculated. This is the combination of the DVA and RUA using theorem of pythagoras.

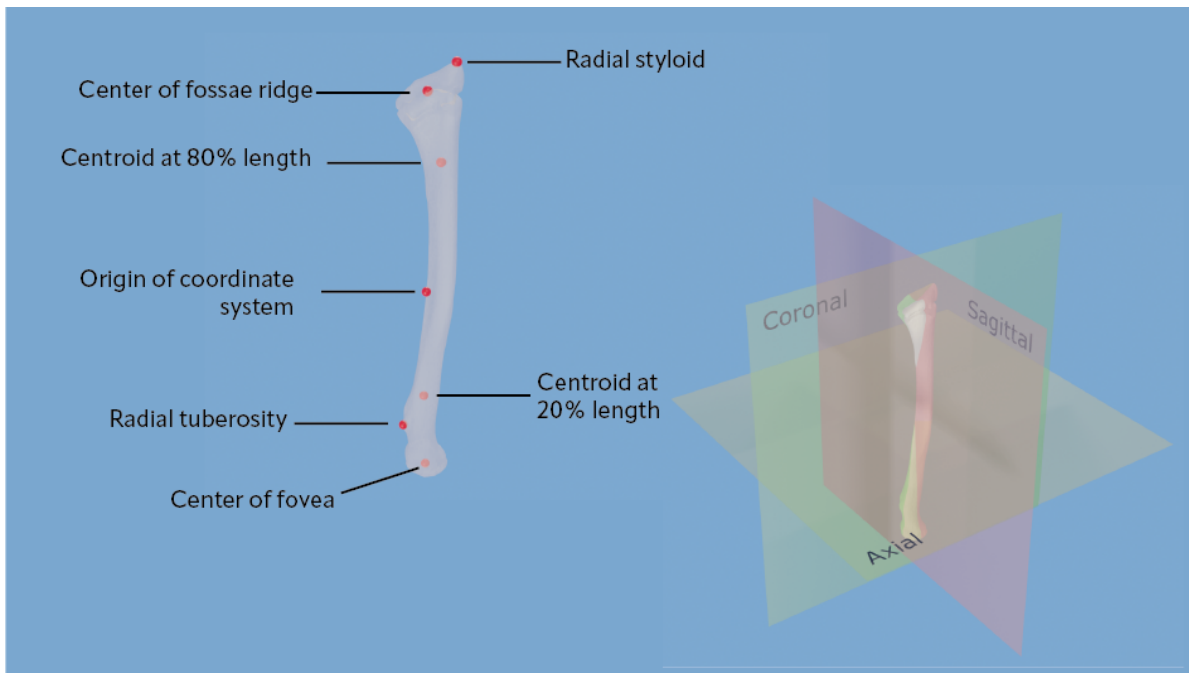


Figure 2.1: Left: anatomical landmarks used for a radius bone. Right: anatomical planes based on landmarks

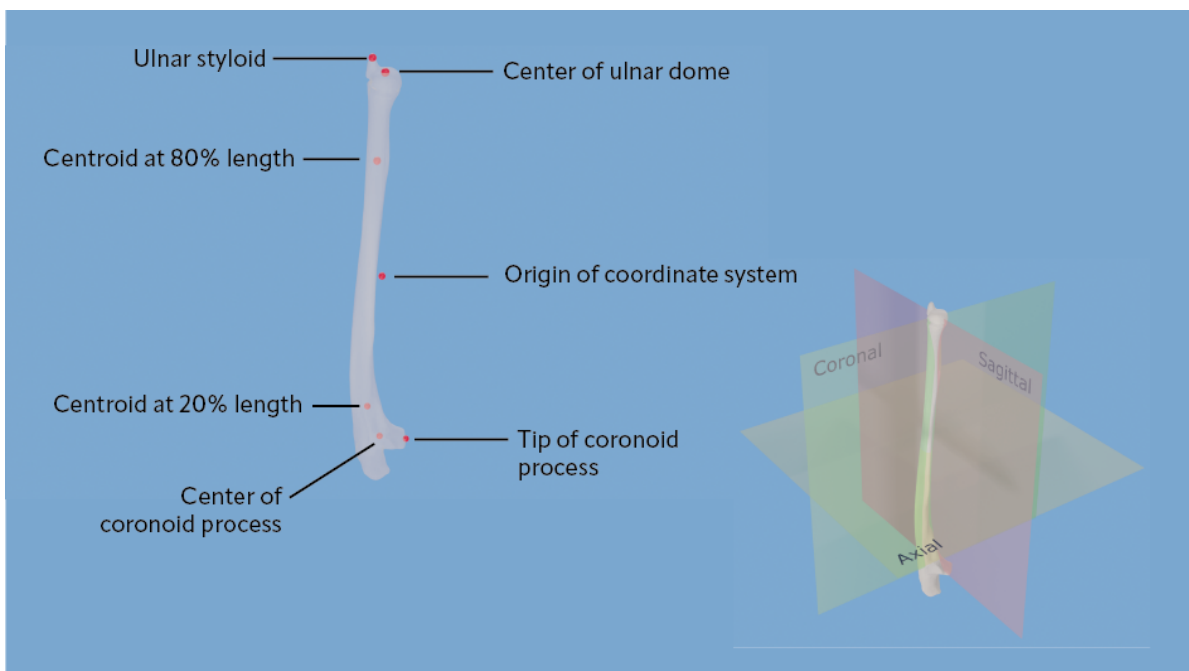


Figure 2.2: Left: anatomical landmarks used for a ulna. Right: anatomical planes based on landmarks

2.2.3. Grouping patients

Based on the direction of the angulation, the patients are grouped. One group is angulated in the positive direction, the other group in the negative direction. This is done for the both bones (radius and ulna) in each of the three directions (DVA, RUA, IA). The mean loss of function (pronation, supination, full range) of the positive group is compared to the loss of function of the negative group. Three losses in three directions means that nine comparisons are made for each bone, which leads to eighteen comparisons in total.

Patients are also grouped based on their loss of function in either pronation or supination function. One group holds the patients with a predominant loss of pronation, the other group holds the patients with a predominant loss of supination. The four measurements of angulation are then compared between the two groups for the both bones, which leads to sixteen comparisons in total.

2.2.4. Statistical calculations

The four deformity measurements were correlated to the loss of pronation, supination and full arc. Pearsons correlation coefficient (r) for each of the 24 correlations (loss of pronation, supination, full arc versus DVA, RUA, IA, TA for the radius and ulna) were calculated. Comparisons between groups as described earlier will be calculated using one-way ANOVA. A result is significant for p-values below 0.05. All calculations are done in SPSS Version 26. [21]

2.3. Results

All the deformity measurements can be found in table A.1. The results between angulation and loss of function can be found in table 2.1. The means and comparisons between dichotomized angulation can be found in table 2.2 and the dichotomized loss of function in table 2.3.

Fifteen patients were included. Mean loss of pronation was 25.34 (SD: 18.58) degrees, mean loss of supination was 61.07 (SD: 22.76) degrees and mean loss of full arc was 86.4 (SD: 20.82) degrees. Most patients had a predominant loss of supination ($n=11$). When looking to the angulations, no volar angulated radii are present in this study: all fifteen are dorsally angulated.

Only three of the 24 correlations are significant ($p<0.05$), all concerning angulation of the ulna. First, radioulnar angulation has a negative linear correlation with loss of pronation, meaning that loss of pronation is more probable with an ulnar angulation of the ulna. Second, the internal angulation of the ulna is correlated with loss of supination, meaning that a loss of supination is more common in forearms with a pronation angulated ulna. Third, loss of the full arc is correlated with the true angulation of the ulna, meaning that a larger true angulation is seen with a larger loss of the full range of motion. These correlations are visualized in figures 2.4.

The loss of pronation because of an ulnar or supination angulated ulna can also be found from the dichotomized angulations and dichotomized function loss. The loss of pronation is significantly larger in the group with an ulnar angulation, while for the loss of supination the ulna is angulated in the radial direction. This is also true for dichotomized loss of function: the group with a larger pronation loss shows on average an larger angulation in the ulnar direction, while the group with a supination loss have a larger angulation in the radial direction. The loss of pronation is also seen more often in combination with a supination angulated ulna

2.4. Discussion

The research question was if the direction of angulation of the radius and/or ulna is predictive for the rotational limitation in patients with a diaphyseal malunited fracture. From this research it can be concluded that the radio-ulnar and internal angulation of the ulna does say something about the final rotational deficit, but this effect is unsure. A loss of supination is seen in combination with a pronation angulated ulna and the total angulation shows a positive correlation with loss of the full range of motion. Most important however is the direction of angulation of the ulna in the coronal plane: ulnar angulation is seen more often in combination with a loss of pronation, while a radial angulation is often seen in combination with a loss of supination.

Two main disadvantages are present in this study. First, there is no correction done for multiple testing. For example, the p-value between the groups based on angulation (24) would lead to a significant threshold of 0.002 with a Bonferroni adjustment. No finding would be significant in this way. The best way to compare all these values would be a multiple regression, but this is also where the second disadvantage comes in: the number of patients is small. This makes the results less strong.

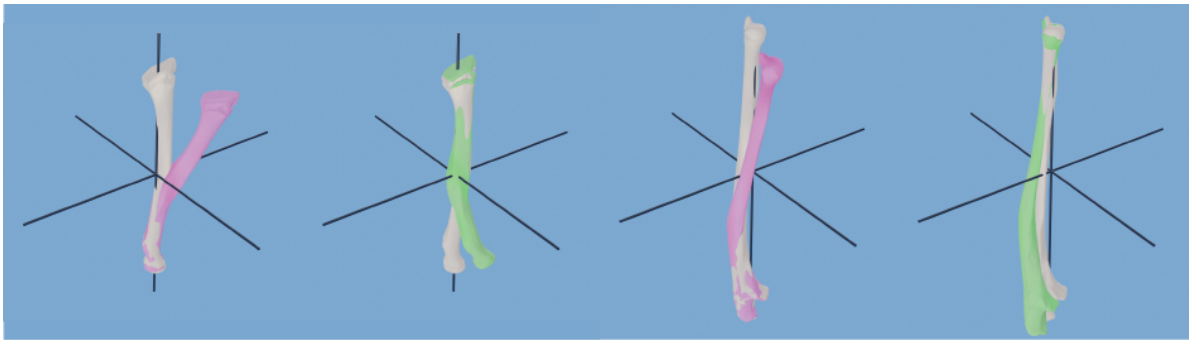


Figure 2.3: Proximal alignment of affected bone (green/purple) on mirrored unaffected bone (white). Left: proximal alignment radius. Middle left: distal alignment radius. Middle right: proximal alignment ulna. Right: distal alignment ulna.

		Pronation loss	Supination loss	Full range loss
Radius	DVA	-0.024	0.171	0.165
	RUA	0.262	-0.305	-0.099
	IA	0.072	-0.139	-0.088
	TA	0.336	0.048	0.352
Ulna	DVA	0.327	-0.211	0.062
	RUA	-0.590*	0.327	-0.170
	IA	-0.277	0.589*	0.396
	TA	0.390	0.186	0.552*

Table 2.1: Pearsons *r* for each correlation between angulation measurement and loss of function compared to contralateral side.

*Statistical significance $p < 0.05$

**Statistical significance $p < 0.01$

		Mean loss of pronation (SD)	Mean loss of supination (SD)	Mean loss of full range (SD)
Radius	Dorsal (n=15)	25.3 (19.2)	61.1 (23.6)	86.4 (21.5)
	Volar (n=0)	NA	NA	NA
	Radial (n=8)	31.5 (13.1)	53.9 (26.2)	85.4 (22.4)
	Ulnar (n=7)	18.3 (23.5)	69.3 (18.6)	87.6 (22.3)
	Pronation (n=10)	22.8 (15.3)	61.7 (25.3)	84.5 (21.1)
	Supination (n=5)	30.4 (26.9)	59.8 (22.4)	90.2 (24.5)
Ulna	Dorsal (n=6)	33.0 (25.6)	54.7 (30.6)	87.7 (27.6)
	Volar (n=9)	20.2 (12.8)	65.3 (18.3)	85.6 (18.3)
	Radial (n=12)	19.6 (15.0)*	68.4 (19.0)*	88.0 (18.7)
	Ulnar (n=3)	48.3 (18.9)*	31.7 (16.5)*	80.0 (35.3)
	Pronation (n=10)	23.0 (19.7)	65.6 (19.6)	88.3 (19.7)
	Supination (n=5)	31.8 (19.0)	48.5 (31.9)	80.3 (28.3)

Table 2.2: Patients grouped based on positive (dorsal, radial, pronation) angulation or negative (volar, ulnar, supination) angulation of radius and ulna. Mean loss in pronation, supination and full arc given.

*Statistical significance $p < 0.05$

**Statistical significance $p < 0.01$

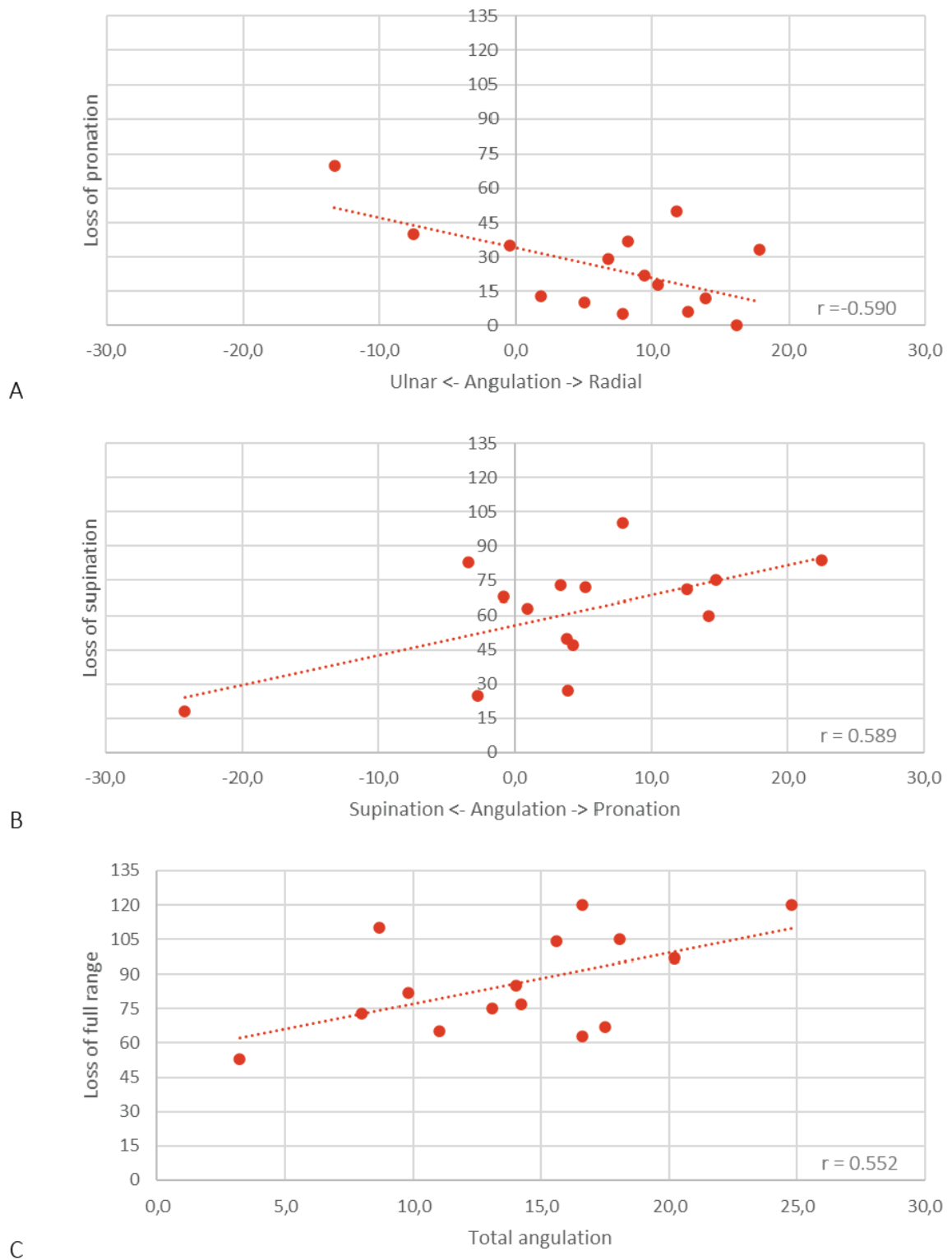


Figure 2.4: Significant correlations between loss of function and angulation. (A) A negative correlation between loss of pronation and radio-ulnar angulation of the ulna, meaning that a pronation loss is more common when the ulna is angulated in the ulnar direction. (B) A positive correlation between loss of supination and internal angulation of the ulna, meaning that a supination loss is more common with pronation angulation of the ulna. (C) A positive correlation between total angulation of the ulna and a loss of the total range of motion.

		Mean angulation with prominent pronation loss (SD) (n=4)	Mean angulation with prominent supination loss (SD) (n=11)
Radius	DVA	12.1 (8.1)	15.9 (5.9)
	RVA	4.6 (12.0)	1.2 (6.9)
	IA	8.4 (30.3)	7.3 (16.0)
	TA	17.1 (6.5)	17.1 (6.3)
Ulna	DVA	3.5 (15.1)	-4.7 (8.4)
	RUA	-2.4 (10.8)**	10.0 (4.8)**
	IA	-4.8 (13.3)*	7.4 (7.8)*
	TA	14.7 (9.0)	13.9 (4.0)

Table 2.3: Patients grouped based on more prominent pronation or supination loss compared to contralateral function. Mean angulation in each plane given.

*Statistical significance $p < 0.05$

**Statistical significance $p < 0.01$

	Radius	Ulna
DVA	DA correlates negatively with range of pronation [1] DVA correlates positively with loss of full range [34]	No findings
RUA	No findings	RUA correlates negatively with range of supination [1] RUA correlates positively with loss of supination [34] RUA correlates positively with loss of full range [34] RUA correlates negatively with loss of pronation [This research]
IA	No findings	IA correlates negatively with loss of pronation [34] IA correlates positively with loss of supination [This research]

Table 2.4: Found significant correlations of this and comparable studies between angulation and rotational restriction.

The findings of this study and comparable studies from Abe et al. and Miyake et al. are combined in table 2.4. In this study for the radius no link between angulation and limitation could be found. The reason could be the absence of patients with a volar angulated radius. This deformation is not seen often in the other studies as well: only Miyake et al. have three patients with a volar angulated radius but does not find a link with rotational restriction [34]. The lack of volar angulated radii is probably because most diaphyseal fractures occur after a fall on a stretched forearm which leads to bones pointing in the volar direction. When reduction is inadequate this will lead to a dorsal angulation. Abe et al. does find that a larger dorsal angulation of the radius leads to a larger restriction of pronation [1].

The results concerning the angulation of the ulna are all in line with each other. The RUA correlates negatively with the loss of pronation as found by this study and Miyake et al. found that RUA correlates positively with the loss of supination [34]. For the internal angulation we found a positive correlation with loss of supination and Miyake et al. finds a negative correlation with loss of pronation [34]. This is as expected: the direction of the angulation is then in both directions of angulation predictive of one kind of rotation loss.

This leaves the internal angulation of the bones. The findings of Miyake et al. and this study are in line with each other and the most cadaver studies done on this subject: an internal angulation leads to a deficit in the opposite direction. [24, 57, 52] About the magnitude of the rotational loss and when this occurs the results are unambiguous. Some of the cadaver studies mention that an internal angulation up to 20 degrees leads to an increase in the same direction as the angulation and a loss in the other direction, but this effect is hard to see in patients. [57] Kasten et al. describes that this threshold is at 30 degrees. [24] Another finding points out that the largest limitation from IA will occur if the radius and ulna are rotated in the opposite direction. [15]



Figure 2.5: Examples of how deformity works relative to an unaffected bone. Left: a ulna in pink, proximal aligned shows a volar and radial angulation. This means that when the bone is in normal position, the red ulna, the apex is pointed towards the volar and ulnar direction. Right: a radius bone angulated in the dorsal and radial direction. The apex points towards the volar and ulnar direction, as can be seen by the red bone.

It is however difficult to apply these findings to patients because the effect is only seen from a large internal angulation and this angulation does often not occur isolated.

3

Kinematic model of pronation and supination of the forearm

3.1. Introduction

Forearm pronation and supination is possible because of the specific shape of the radius and ulna: there is space for the radius to lay over the ulna during pronation [51]. At the same time it is known that the central band is isometric and its length normally does not change during rotation [36]. To visualize bone movement and measure central band length, the rotational movement of the radius and ulna must be retrieved. Dynamic CT is a possibility, but the limited field-of-view, relative low resolution and radiation are disadvantages for this technique. [22, 9] Another possibility would be to model the movement of the patient specific bone surface models. This would lead to a specific rotation of the radius and ulna of that patient and anatomy and a possibility to identify bone impingement and measure the central band length and bone distance.

This chapter describes how the movement of the radius during pronation and supination in unaffected forearms is modeled and how distance can be measured. Then, this model is validated using cadaveric scans. The position of the modeled radius and radius of the specimen are compared. Aim is to develop a kinematic model which can model pronation and supination by minimizing translation based on the bone surface models of the radius and ulna.

3.2. Method

All code is written in Python 3.8.11. [59] For mesh and point cloud calculations the library of Trimesh is used, version 3.9.31. [14] The meshes undergo the same subdivision filtering as mentioned in chapter 2. In the model the ulna is aligned following the coordinate system mentioned in chapter 2. All directions and planes are therefore relative to the ulna.

3.2.1. General working principle of the rotation

The kinematic model in this research will focus on the movement of the radius relative to the ulna. That means that the ulna will be fixed during rotation. The kinematic model rotates the radius around a line from the proximal radial head to the distal ulnar head. The proximal radio-ulnar joint (PRUJ) determines the proximal rotation point and the distal radio-ulnar joint (DRUJ) the distal rotation point. A floating axis will be used: the rotational points in the PRUJ and DRUJ will move to keep the distance in these joints constant and to minimize translation of the radius.

To measure the course of the central band during rotation, multiple positions of the radius must be modeled. This means that to reach a certain position of s_t degrees from the initial position of the bone surface models, smaller rotations of s_n degrees must be modeled. The number of steps n is an integer and given by $n = s_t/s_n$. First, from the bone surface models as extracted from the CT-scan the initial rotation axis is determined. In the PRUJ the centroid of the most proximal 5% of the radial surface model is used. In the DRUJ it is the centroid of most distal 5% of the ulnar surface model. Second, along this axis a rotation of s_n degrees is applied to the radius. Third, the distance of the radius relative to the ulna is considered. Following rules explained below the point of rotation in the DRUJ and PRUJ are translated, tilting the rotational axis. This is

repeated until all n steps are applied and in total an angle of s_r is applied.

The value for s_n is usually between 1 and 10 degrees. To calculate the position of the radius for higher values of pronation and supination multiple smaller rotations are applied after each other. That means that for example a rotation of +60 degrees is being modeled this is done by applying 12 rotations of +5 degrees. For each rotation the separate rotational axis is calculated and the rotation is applied. From this position the next axis is calculated and so on, until the target rotation is reached.

3.2.2. Proximal radio-ulnar joint

In the PRUJ, the proximal radial head rotates in the radial notch of the ulna and stays in place because of the annular ligament fixed on the ulna and wrapped around the radial head. Because of this fixation, the assumption is made that the distance between the radial notch and the radial head is constant during rotation. This intra-articular distance is kept constant by creating a line between the center of the radial notch and the centroid of the radial head bone surface model. The radial head is considered to be the most proximal 5% length of the radius. Along this line the centroid of the radial head can move towards or away from the radial notch to increase or decrease the distance. Because the centroid of the radial head must stay on this line, the rotational point is calculated based on the initial position of the centroid and the calculated position of the centroid to keep the distance the same.

3.2.3. Distal radio-ulnar joint

The DRUJ can not be considered in the same way as the PRUJ because of the irregular shape of the distal radius and ulnar head, which shows much more patient specific anatomy than the joint surfaces of the PRUJ. Not only there are notches radial and ulnar of the ulnar styloid, but often the epiphyseal plate is not yet completely closed in younger patients, which is the main patient population for diaphyseal fractures. To make the same assumption that the intra-articular distance is kept constant during rotation, the shape of the ulnar head must be simplified. This is done using an ellipsoid: a sphere of which its three axes are not the same. By fitting an ellipsoid around the ulnar head, the surface becomes regular and distance can be kept constant.

On the most distal 5% to 3% of the ulna the minimal volume ellipsoid is fitted. The distal tip of the ulna is excluded to reduce anatomical variation in the ulnar styloid. The centroid of the sphere is the initial distal rotation point, comparable with the centroid of the proximal radial head in the PRUJ. From the sphere the ellipse which expands in the dorsovolar and radioulnar direction is kept. Because of the shape of the ulnar head the short axis of this ellipse runs in the radioulnar direction and the long axis in the dorsovolar direction. In this ellipse the rotation point moves along a line on the short axis of the ellipse, comparable to the centroid of the proximal radial head in the PRUJ.

The desired effect is to reduce the distance between the distal radius and ulnar head in the higher values of pronation and supination. In these positions the distal radius is positioned either radial (supination) or ulnar (pronation) relative to the ulnar head. In normal joint kinematics the distal radius is pulled towards the ulnar head by the distal radio-ulnar ligaments. By moving the rotational point along the short axis of the ellipse, this effect is mimicked. The position of the center of the ulnar notch relative to this line determines how much the rotational point moves along this axis. When the center of the ulnar notch is positioned on the radial or ulnar end of the line, the pulling effect is the strongest. Positions in between will be logarithmic interpolated: the size of the steps will decrease from volar to radial and ulnar. This means that the pulling effect is stronger when the radial head is at the volar side of the ulna and pronates or supinates.

3.2.4. Validation

The modeled position of the radius is validated using scans of cadaveric arms. CT-scans of two specimens are made in 90, 60, 30 degrees of pronation, supination and in the neutral position. After segmentation and conversion to bone surface models, the forearm scanned in neutral position is used to model forearm rotation. Rotation from -100 to + 100 degrees is modeled in steps of 1 degree.

The ulna of the neutral scan is used to position the forearm in the center of the coordinate system. A scan in a certain position, for example 90 degrees supination, is then imported and the bone surface model of this ulna is registered on the ulna of the neutral position. The radius of the neutral position and the radius of the 90 degrees pronated radius are different. The rotation angle that is needed to rotate the radius in neutral position to the pronated radius is calculated. This angle is then modeled, see figure 3.4. The rotational axis as unit vector, Euler angles, and center of rotation of the applied transformation from neutral position to pronated or supinated position is calculated for the specimen scans and the model and compared.

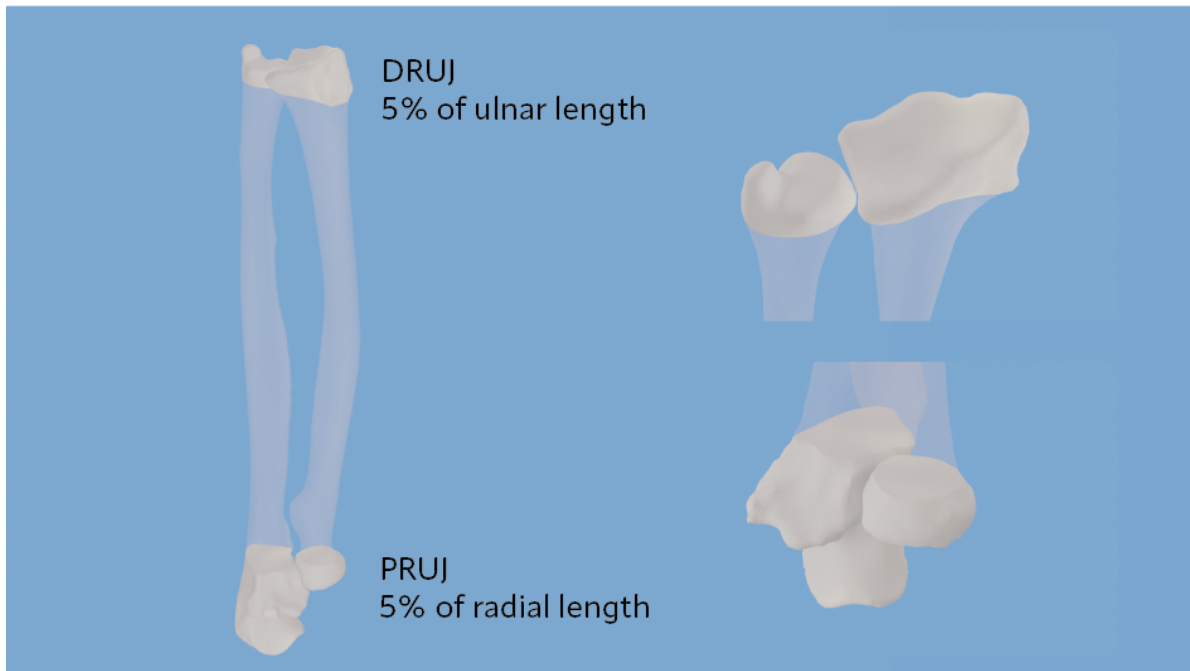


Figure 3.1: Identifying the joints in the forearms. The proximal radio-ulnar joint is considered to be the most proximal 5% of the length of the radius. The ulna is sectioned at the same length. The same idea is used in the distal radio-ulnar joint: the distal 5% of the ulnar length is used and the radius is sectioned at this length as well.

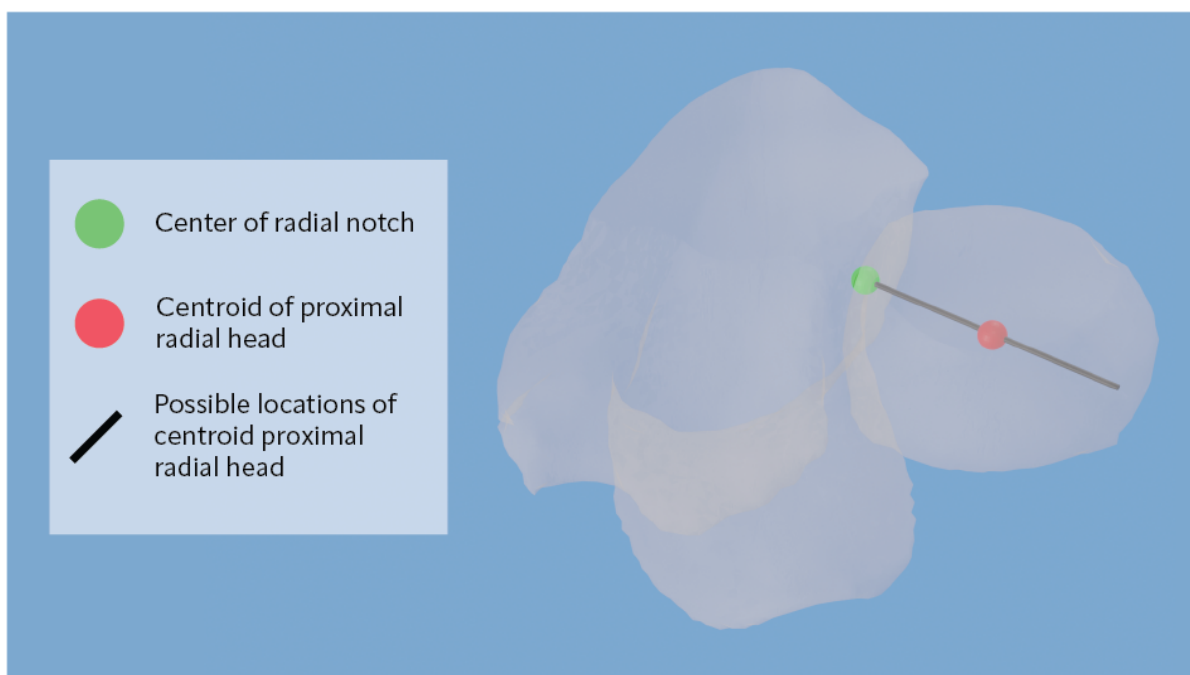


Figure 3.2: The proximal radio-ulnar joint and how the proximal rotation point is calculated. The assumption is that the radial head has one degree of freedom: it can move towards and away from the center of the radial notch. This means that the centroid of the radial head (red) must stay on the black line. By calculating the new position of the centroid in order to keep the distance between the joint surfaces equal, the proximal rotation point can be calculated using the angle of rotation applied and the distance between the initial position and new position of the centroid.

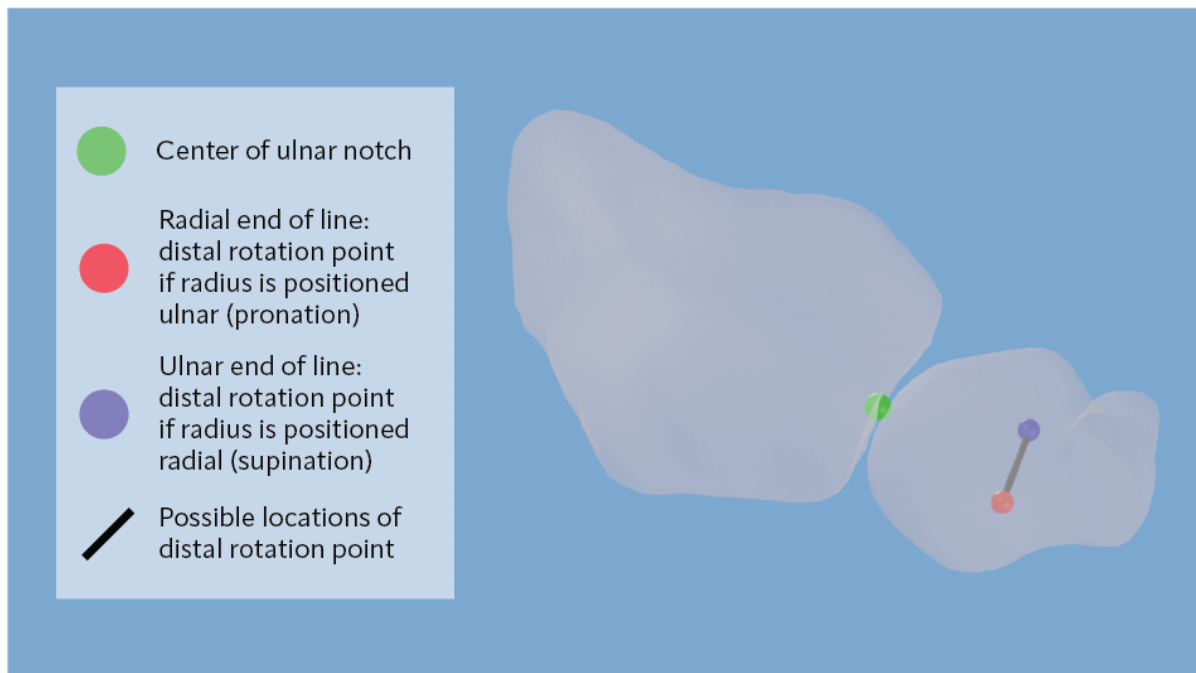


Figure 3.3: The distal radio-ulnar joint and how the distal rotation point is calculated. The assumption is that the distal radius must move towards the ulnar head when positioned ulnar or radial of the ulnar head. To reach this position an ellipsoid is fitted. The difference in length between the long axis and short axis is the distance the rotational point can move along the short axis. When the distal radius is ulnar relative to the ulna, so the forearm is in pronation, the rotation point is located at the most radial side of the line and vice versa.

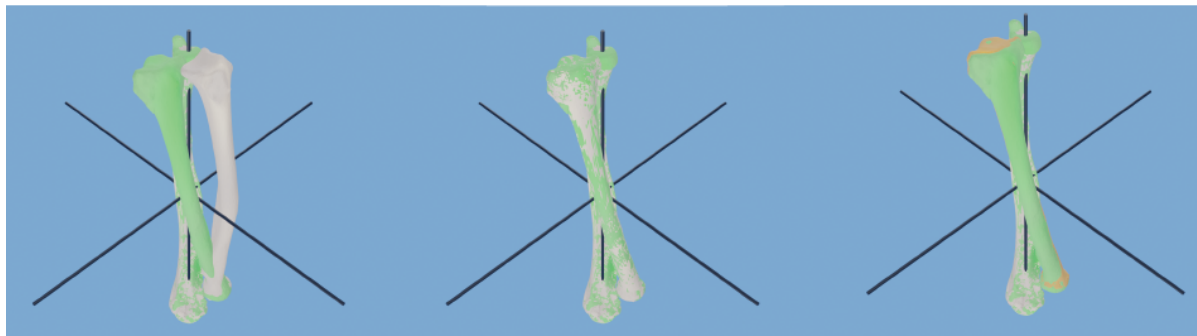


Figure 3.4: Validation of the model on a specimen scanned in 90 degrees of pronation. The white models correspond to the specimen scanned in neutral position, the green models correspond to the specimen scanned in 90 degrees of pronation, the orange model corresponds with the modeled position of the radius. Left: the ulna of the rotated specimen is registered with the ulna in neutral position: in this way these overlap and the difference in position of the radius can be seen. Middle: the radius in neutral position is registered to the radius in 90 degrees pronation. From the applied transformation the angle of rotation is calculated. Right: the radius is modeled with an endpoint at the calculated angle of rotation.

Direction	Dorsovolar	Radioulnar	Internal
Mean rotation error (degree)	0,25	-0,13	0,00
Mean translation error (mm)	-0,01	0,01	-0,13

Table 3.1: Mean rotation error given in degrees and translation error given in millimeters for the kinematic model as validated with two specimen in 30, 60 and 90 degrees of pronation and supination.

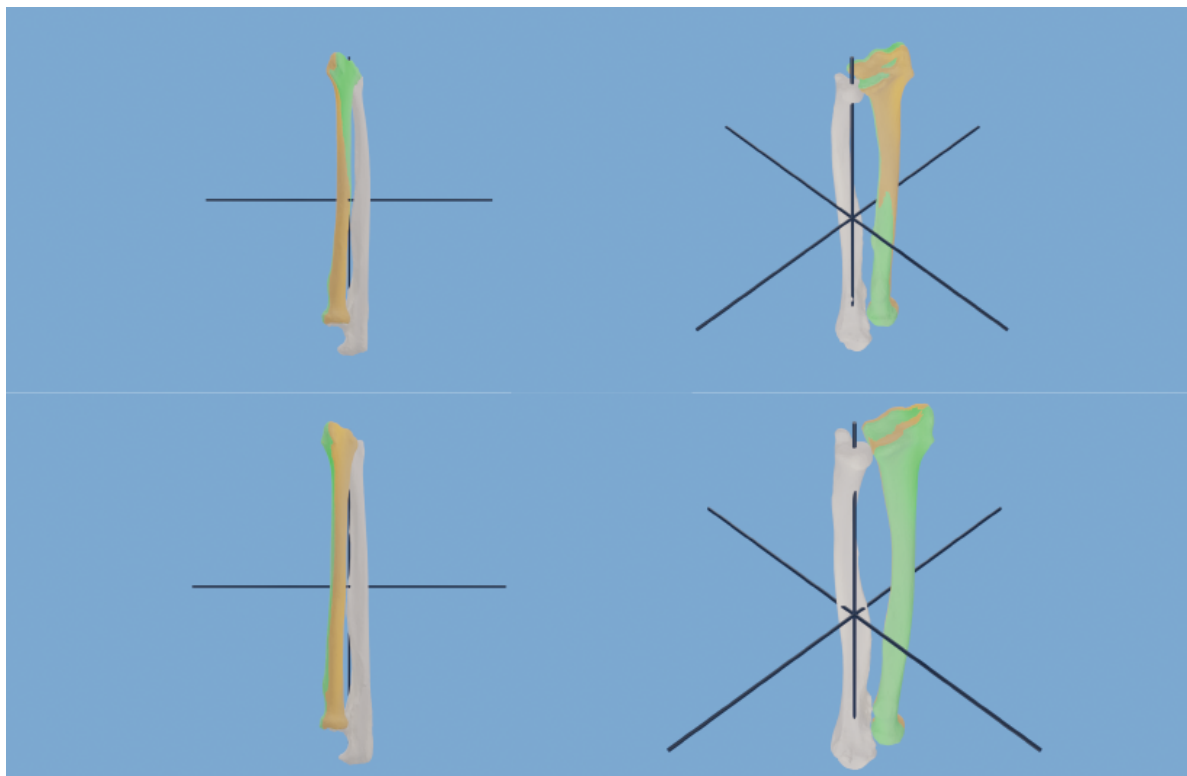


Figure 3.5: Modeled and true position of the radius in 90 degrees supination. Green bone models are from the specimen, orange models from the model. The upper two images are from specimen 1: it can be seen that the radius tilts dorsally distal, but volar proximal. This is the change in angle larger than 1 degree in the sagittal (dorsovolar) plane. The bottom two images are from specimen 4: here can be seen that the radius is moved dorsally, not rotated. The distal and proximal parts are both more dorsal than the model. This error however is less than 1 millimeter.

3.3. Results

Two specimen forearms were scanned and used to model forearm rotation. The mean rotation error and translation error for all locations combined is given in table 3.1 For the three positions of pronation and supination the true and modeled rotation axis, Euler angles and center of rotation are given in appendix B. The applied angles are negative in pronation because it were right forearms. In a rotation the center of rotation is the same as a translation following after a rotation.

In specimen 1 it can be seen that in supination there is more than 1 degree difference in rotation in the radioulnar plane, see figure 3.5. The radius of the specimen shows that in supination the distal radius is located more dorsally, while the radial head stays in place. In specimen 4 this effect is present, but the difference with the modeled position is less than 1 degree. The difference in translation between the specimen and the model is lower than 1 millimeter in each direction. In pronation there is no difference larger than 1 degree in each plane for rotation and also the modeled center of rotation shows no differences larger than 1 millimeter in every direction.

The applied angle and position were different for the two specimens. Especially in pronation the difference between position and rotation angle becomes larger in higher values for pronation. Supination differs less within one specimen, but comparing the two specimens shows that the rotation of the radius in specimen 4 is much smaller in 30 and 60 degrees of supination. The rotation axis is hard to compare between the specimen because it depends on the bone length

3.4. Discussion

The kinematic model as described in this chapter can model radial movement and different positions of the radius with mean errors lower than 1 millimeter and 1 degree. This model can be used to measure bone distance in different positions of the radius. The biggest difference between the cadaveric scans and the model is seen in supination in one of the two specimens. The radius tilts dorsally relative to the ulna, while the proximal radial head moves more volar. This error can be seen in early supination and is not corrected in later positions. It is however not known if this a natural effect of supination: this could also be a result of forcing the specimen in this position.

In the PRUJ the assumption that the distance between the radial notch and the radial head is constant neglects the fact that the cartilage on the radial head has not the same thickness over the full surface. There is less cartilage in the more volar and dorsal parts of the radial head, so therefore the distance between the radial notch and radial head will be smaller in pronation and supination than in the neutral position. [7] Furthermore, the effect of the quadratus ligament, which attaches the radial head to the radial notch is also neglected, but it is unknown what the effect on the kinematics of the radial head are. One cadaveric study points out that dissecting the quadratus ligament increases supination by 10 to 20 degrees and it limits the rotation of the radial head. [56]

The DRUJ is more difficult to model because of the varying shapes of the distal radius and ulnar head and the more complex ligament structures which have an influence on movement of the DRUJ. While the used method does reduce the distance between the ulnar head and radial head in pronation and supination, the validation scans show even more reduction of the distance. This is probably not due to cartilage only present at the volar side of the radius, because cartilage is prominently present on the radial side. [6]. More likely is that the ligaments change the movement of the distal radial head significantly in pronation resulting in rotation not prominently around the longitudinal axis of the forearm. This is found in the most recent study concerning the distal rotation point of the forearm. [2] While the radioulnar translation of the distal rotation point quite constant and does not vary much between individuals, the dorsolvolar translation is different between individuals. Only a volar translation is seen from 70 degrees of supination.

One must also consider the quality and effects of segmentation and smoothing of the bone surface models. Some models showed overlap between the radius and ulna in the scanned position of the PRUJ. This is the reason for the use of rays to calculate the interarticular distance instead of vertices. This lead to an immediate increase in distance from the scanned position to the very next position to compensate for this error.

Next to further validation of this model with the unused six cadaver specimen, the next step would be a dynamic CT-scan of the wrist and elbow. This eliminates the force needed on the specimens to reach and keep certain positions, which will lead to a more natural movement. This must then also be connected to in vivo pronation and supination measurements. From the two used specimen it is possible that the angle of rotation is not equal to the rotational position. As Akhbari et al. points out the rotation point in the DRUJ moves volar in late supination, meaning that a different rotation could be seen [2]. However, a measurement error in pronation and supination position is plausible for positioning the specimen.

4

Bone distance during pronation and supination as measured from a kinematic model

4.1. Introduction

Rotational movement of the forearm is needed in many activities of daily living. Average range of pronation and supination of the forearm is respectively about 75 and 85 degrees [37]. For the most daily activities, a range of 50 degrees pro- and supination is sufficient [18]. However, some more recent research pointed out there are some more contemporary tasks, such as the use of a mobile phone and typing, which require more pronation [49, 58]. A rotational restriction in the forearm can therefore have multiple drawbacks. Compensation with other movements is possible, but this can lead to pain in the long term. In children, limitation can impede development and learning.

Patients with a malunion of the radius, ulna or both are at risk of developing a rotational restriction [45]. While conservative treatment does lead to good results, malunion is one of the most common complications and leads to a persisting deformity of the radius and or ulna [25, 38]. In some cases a malunion can cause significant disability in pronation and/or supination of the forearm [16]. While it is known that a greater deformity often leads to a larger disability of movement, some patients with smaller deformities still have a limitation of rotation [13, 52, 4, 8]. It is also known that not every patient with a malunion will develop a limitation: it varies among studies between 15 up to 35% [46, 61, 42]. The extent to which bone deformity has an influence on the normal function is unsure.

Recent research found that rotation in patients with a malunited diaphyseal fracture could only be restricted because of two reasons: bone impingement or contracture of the central band [1]. Bone impingement would occur mainly in pronation, contracture of the central band could be seen in supination. The central band is considered the most important ligament in the interosseous membrane, because it is the ligament with the lowest strain between the radius and ulna [27] and it is known that its length does not change significantly during rotation in unaffected forearms [36]. In these studies, the measurements were done by comparing the CT-scans of malunited forearms in maximum supination, neutral position and maximum pronation. Minimal distance between the bones and the length of the central band was measured and compared between these three positions. This would mean that the distance between the radius and ulna is different between a healthy, unaffected forearm and a malunited forearm. To our knowledge, there is no research on this topic available, only the description of the distance between the bones in healthy forearms [10]. This study shows that the distance becomes smaller in pronation, while in supination a small enlargement is seen and then this distance decreases.

Using this knowledge, it would be possible to predict range of motion when bone impingement can be recognized and the length of the central band can be measured. Based on unaffected forearms thresholds for maximal central band enlargement could be set. As a proof of concept, this hypothesis will be tested using a kinematic model. The aim of this research is to predict the range of motion of malunited forearms by recognizing bone impingement and central band length from a kinematic model. The threshold for range of pronation will be set by modeling the rotation of unaffected forearms and look at the change of length of

the central band from neutral position. This threshold will then be used to predict the range of motion of the patients' malunited forearms. Furthermore, it will be tested if the interosseous distance between the radius and ulna is different between patients' affected and unaffected forearm.

4.2. Method

The method consists of four parts. First, the position in which the forearms are scanned must be determined in case this is not the neutral position, otherwise the range of pronation and supination can not be determined. Second, the rotation of unaffected forearms will be modeled and there is checked for bone impingement and the central band length (CBL) and the minimum interosseous distance (MID) is measured. Third, from the CBL in the unaffected forearms a threshold for maximum change of length relative to the neutral position will be set. Fourth, the rotation of malunited forearms will be modeled, bone impingement, CBL and MID are measured and range of pronation and supination will be predicted.

The affected and unaffected forearms of the same fifteen patients as mentioned in chapter 2 are modeled. The kinematic model as described in chapter 3 is used. The rotation is modeled to 100 degrees of pronation and supination in steps of 5 degrees. The maximum value is set to 100 degrees because this is the maximum value measured in vivo on a unaffected forearm, see table A.1.

All code is written in Python 3.8.11. [59] For mesh and point cloud calculations the library of Trimesh is used, version 3.9.31. [14] The meshes undergo the same subdivision filtering as mentioned in chapter 2. In the model the ulna is aligned in the center of the coordinate system as mentioned in chapter 2.

4.2.1. Determining the neutral position

For calculating the relative length and the position of the origin and insertion of the central band, the forearm must be in the neutral position (zero degrees pronation and supination). Because the patients were scanned in prone position with their hands laying on a cushion, the forearms are not scanned in neutral position. It is therefore needed to first determine the neutral position of the unaffected and affected forearm, which is done in two different ways.

The neutral position of the unaffected forearm is determined by comparing the position of the radius of the scanned position to the scan of a specimen forearm. Only the position of the DRUJ is considered, because this is leading in the pronation and supination position. First the distal 20% length of the ulna of the cadaver is registered onto the unaffected ulna with a procrustes alignment followed by a iterative closest point (ICP) registration. Scaling is allowed to compensate for size differences. Then the radius of the unaffected forearm is registered onto the radius of the cadaver. From this transformation the angle is used to calculate the difference in rotation and thus position. While there were two specimen available to average the position, one specimen showed severe arthrosis which is not comparable with the forearms of the patients in this study. Therefore only one specimen was used.

The unaffected forearm in neutral position is then used as model to calculate the neutral position of the affected forearm. This is not done based on the cadaveric scan because the deformity of the bone makes it harder to compare it with another bone. The contralateral bone is then a better comparison. The same method was used as explained earlier. The unaffected forearm must be mirrored on to the sagittal plane.

4.2.2. Bone impingement

Because the kinematic model uses three-dimensional surface models, the bone model of the radius can overlap with the bone model of the ulna. This overlapping would mean in real life that the bones should have touched and movement should be blocked or altered. When this happens, this is considered as bone impingement as (1) this effect is seen in the diaphyses of the bones and (2) the intersecting volume is at least 5 cubic millimeters to compensate for measurement errors. The region of the diaphysis is determined by slicing of the PRUJ and DRUJ of the bones. This is the radius and ulna sliced proximally at 5% of the radial length and sliced distally at 5% of the ulnar length when the ulna is positioned in the coordinate system as mentioned in chapter 2.

4.2.3. Central band length

In neutral position, the origin and insertion of the central band is located on the radius and ulna. This is done based on a cadaver study from Noda et al. in which the relative height is reported where the ligaments attach to the bones [41]. On the ulna the central band attaches at 56% and 71% of the height as measured from the proximal side, with the center being at 63.5% of the length. On the radius the central band attaches at 36% and

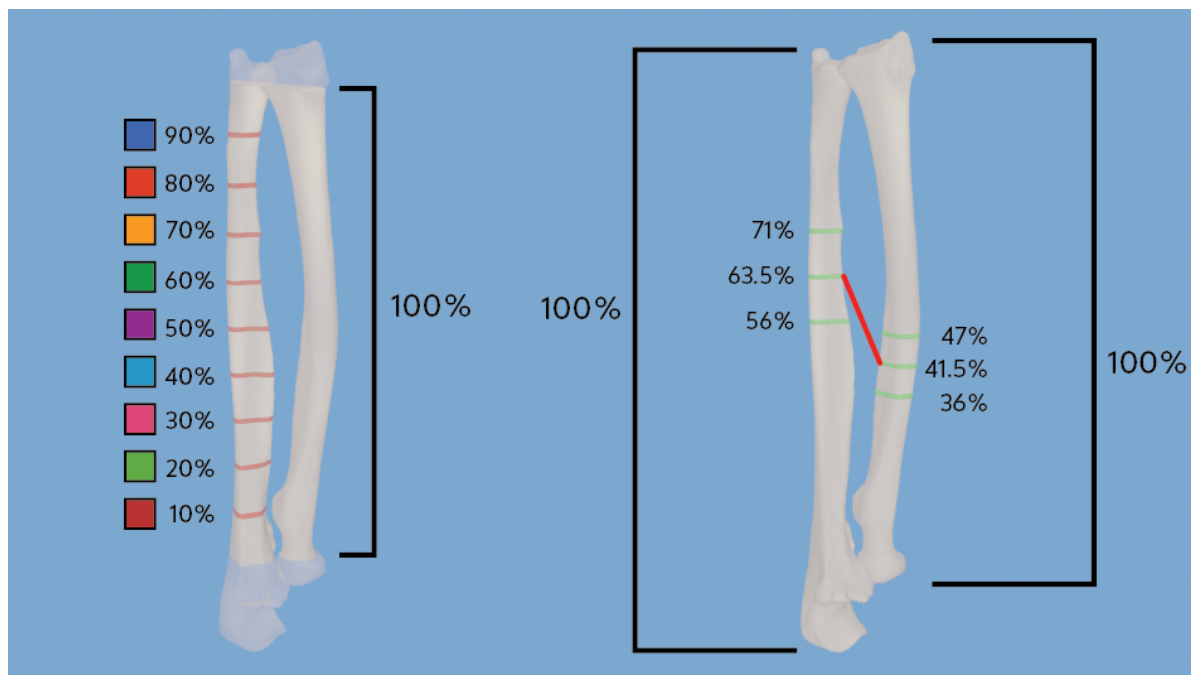


Figure 4.1: Visualizing distance measurements. Left: minimal distance along the length of the ulna. Nine distances are measured by slicing of the 5% most proximal part of the radius and the 5% most distal part of the ulna. Along the surface that is left cross-sections each 10% percent are made and the minimal distance from each cross-section to each position of the radius is measured. Right: how the position of the central band is determined. In neutral position cross-sections at 63.5% of the length of the ulna and at 41.5% of the length of the radius are made. The vertices with the shortest distance is measured and landmarks are placed. During rotation the distance between the landmarks is measured.

47% of the length, with the center being at 41.5%. At the heights of the center cross-sections are made from the radius and ulna horizontal cross-sections are made. These cross-sections consist of vertices, just as the bone surface models. Using euclidean distance the smallest distance between a vertex of the cross-section of the ulna to the vertex on the cross-section of the radius are used as landmarks. The vertices marking the landmarks do not change during rotation in contrast to the vertices defining the MID. Only the length between the centers of the origin and insertion of the central band is measured during rotation. The CBL is also expressed relative to the length in neutral position and is called the relative central band length CBLR. This is done to correct for differences in sizes of the forearm between patients and to make measurements comparable.

4.2.4. Minimum interosseous distance

In the diaphyseal surface model as described in the paragraph for bone impingement horizontal cross-sections are made along the longitudinal length of the bone in steps of 10%, starting at 10% of the length and ending on 90%. Using euclidean distance, the shortest distance between each of the cross-sections and the radius is calculated and is considered as the MID. Again, not only the absolute MIDs are calculated, but also relative to the MID in the neutral position (MIDR).

4.2.5. Statistical tests

The CBL, CBLR, MID and MIDR are compared between the unaffected forearm and unaffected forearms using paired t-tests. For the MID and MIDR this will be done for each of the nine locations and the mean distance of the nine locations. The level of significance was defined as $p < 0.05$.

4.2.6. Predicting range of motion of unaffected forearms

As hypothesized rotation could be blocked due to contracture of the central band or bone impingement. To predict range of motion, a maximal CBLR will be set based on the measurements on unaffected forearms. A relative value is used instead of an absolute value to use one threshold between all patients, independent of patient age and bone size. Based on these two conditions pronation, supination and full arc will be predicted

for all patients. Difference between the model and the in vivo range of motion is given by the root mean square error (RMSE).

4.3. Results

For each patient the unaffected and affected forearm measurements are presented in graphs in the appendix. In these graphs the course of the mean, minimal and maximal MIDR, the CBLR during rotation is visualized and the region in which bone impingement occurs is marked. For the MIDR the values measured at 10% and 90% are not visualized. As explained later, the MIDR values are not significant between affected and unaffected forearms, probably due to anatomical reasons. Furthermore, the patients range of motion for pronation and supination and in affected forearms the predicted range of motion is shown.

4.3.1. Minimum interosseous distance and bone impingement

The MID and MIDR as measured in maximum supination and pronation for all forearms is visualized in figure 4.2. The figures show that the minimal distance between a normal forearm and malunited forearm differs significantly at several locations along length of the forearm in pronation. Affected forearms show that the radius is much closer to the ulna than in the unaffected forearms. The relative measurements show lower p-values than the absolute measurements, probably because bone length is a factor in minimum distance that can be reached. In pronation however, seven out of fifteen patients showed bone impingement at the position that would be reachable following the in vivo measurements. Because euclidean distance is used, the MID values do not show if bone impingement occurs and the minimal distance is still measured. For the unaffected forearms, none of the bones showed bone impingement before the in vivo measured range of pronation. In supination direction none of the forearms showed bone impingement.

In pronation the MIDR showed two measurements which are not significant. This is at the 10% and 90% height. Proximally this is probably because the radial tuberosity extending from the cylindrical shape of the radius, heavily influencing the distance between the radius and ulna. This is probably also why in supination large outliers are visible for this height. Distally the height is too close to the distal radioulnar joint, meaning that the distance naturally will become smaller and is thus not different between affected and unaffected forearms.

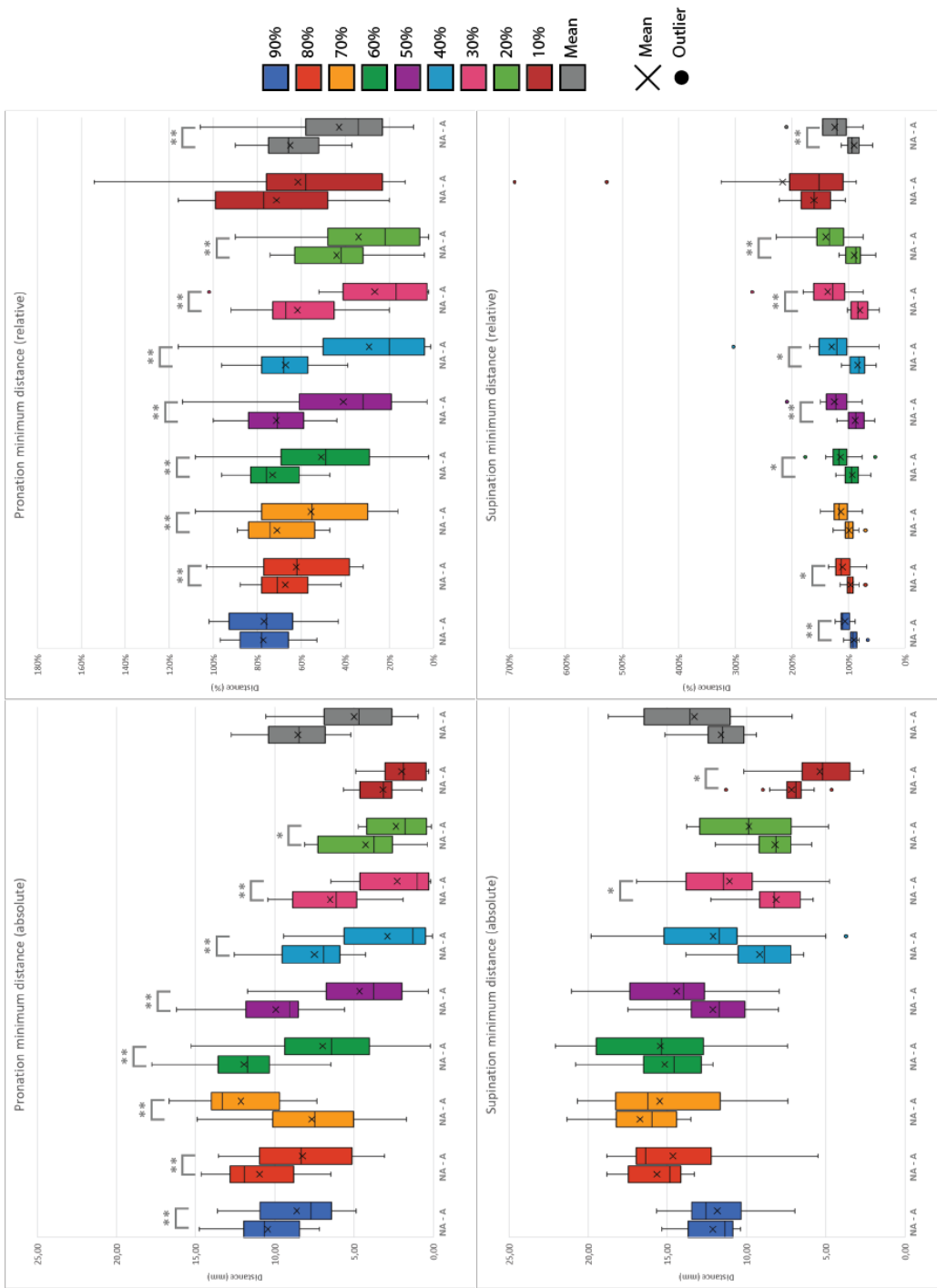


Figure 4.2: Box-and-whisker plots of the distances measured at maximum pronation, supination, absolute and relative to the neutral position of the forearm along the length of the ulna starting at 90% and ending at 10%. Box plot at the end is the mean distance along the diaphysis. For each height the unaffected forearm is placed next to the affected forearm. Statistics calculated with paired t-tests.

*Statistical significance $p < 0.05$

**Statistical significance $p < 0.01$

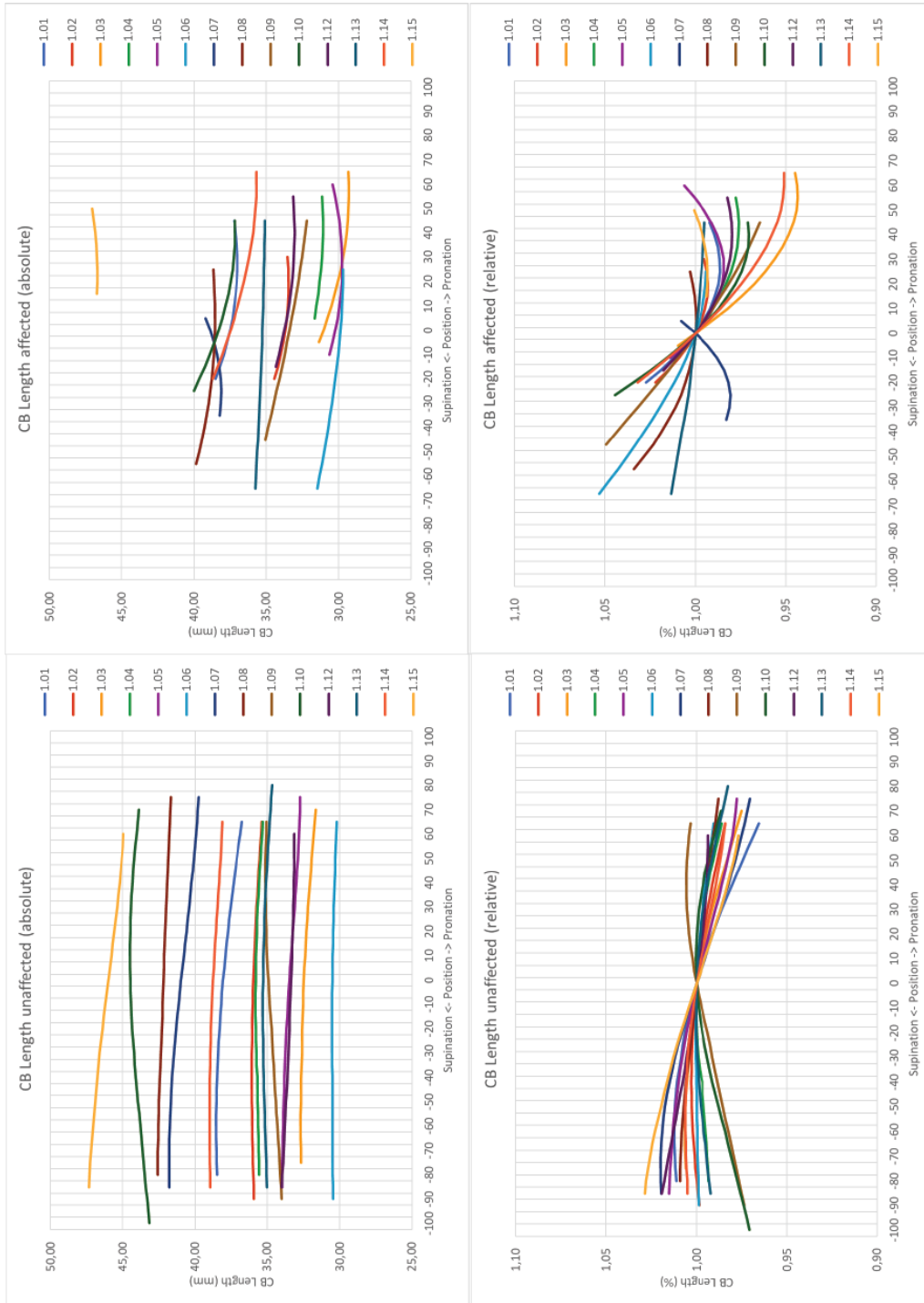


Figure 4.3: Length of the central band during rotation of all 15 patients. Absolute lengths of central band in upper two images, relative length in the bottom two images. Graphs on the left show the unaffected forearms, graphs on the right show the central band of the affected forearms.

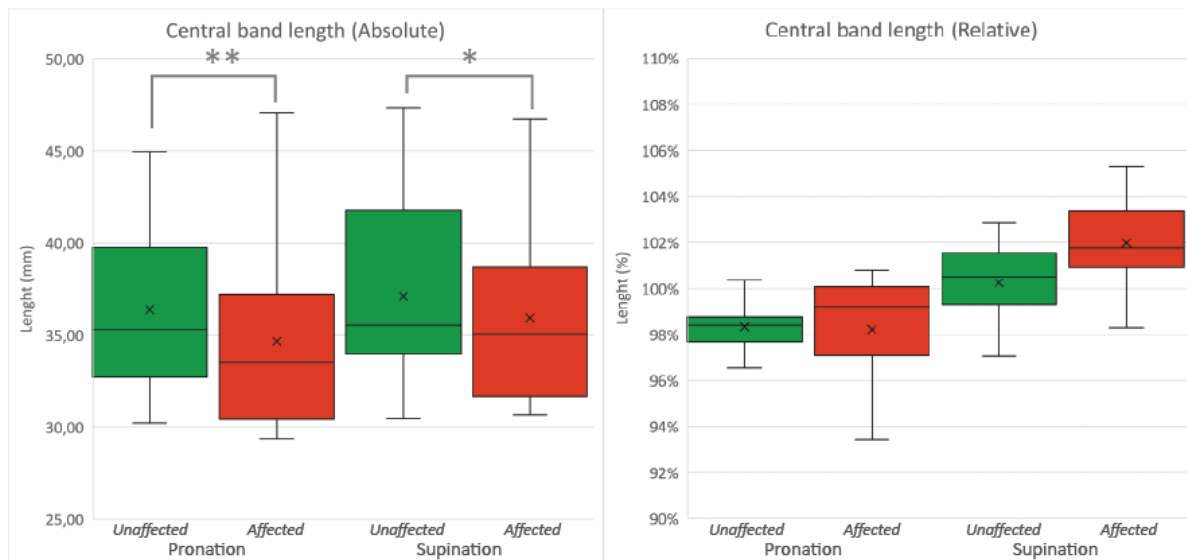


Figure 4.4: Length of the central band at maximum pronation and supination, absolute and relative to the length in neutral position. Upper row: all forearms combined. Middle row: only forearms with a radial angulated ulna. Bottom row: only forearms with an ulnar angulated ulna. Statistics calculated with paired t-tests.

*Statistical significance $p < 0.05$

**Statistical significance $p < 0.01$

4.3.2. Central band length

The length of the central band during rotation in all forearms is visualized in figure 4.3. As can be seen from these figures: the length of the central band does not change much during rotation in unaffected forearms, while in the affected forearms the length increases during supination in most forearms. Only patient 1.07 and 1.13 show different effects. In patient 1.07 the central band extends in length in pronation and decreases in supination. Patient 1.13 has a central band which stays constant during rotation. If compared in the same way as the minimal distances however, see figure 4.4, it can be seen that only the absolute length of the central band differs significantly between affected and unaffected forearms.

4.3.3. Prediction of range of motion in affected forearms

The predicted and in-vivo measured values for pronation, supination and full range of motion for all affected forearms are presented in table 4.1. Positive values indicate pronation, negative values indicate supination. The threshold for maximum CBLR is set at 103%, which is the largest value measured in the unaffected forearms as can be seen in figure 4.3. Pronation was predicted because of bone impingement for every patient and supination could be predicted because of CBLR. Only once, for patient 1.13, supination was not limited because of the central band; the length stayed constant, just like the unaffected forearms. Therefore the range of supination of the unaffected forearm of this patient was used as prediction.

Two patients, 1.04 and 1.15, lost their full range of supination and could not reach the neutral position. Because the model does not keep this into account, the radius is moved to a position which is for the patient not reachable. On forehand it is known that the predictions for these patients will be wrong. The RMSE is therefore calculated including and excluding these cases. The RMSE becomes smaller when these cases are excluded: 19.4 degrees becomes 15.2 degrees. Also the prediction of the full range improves: 24.8 degrees versus 17.9 degrees. The effect on the pronation prediction is much lower: 17.6 degrees versus 17.0 degrees.

4.4. Discussion

By modeling pronation and supination of the forearm the range of motion of malunited forearms can be predicted with a relative mean squared error of 17.9 degrees only based on bone impingement and the relative length of the central band. MIDR is different for the 20% to 80% of the length of the bone between affected and unaffected forearms in pronation. However the measured values for pronation in the affected forearms showed bone impingement in the kinematic model, which makes these MID measurements not very useful. It does show however that bone impingement is probably the reason for a limited range of pronation: this

	Pronation		Supination		Full range	
	In vivo	Predicted	In vivo	Predicted	In vivo	Predicted
1.01	45	40	-20	-20	65	60
1.02	30	15	-20	-25	50	40
1.03	65	50	-5	-25	70	75
1.04	55	85	5	-20	50	105
1.05	60	25	-10	-20	70	45
1.06	25	40	-65	-45	90	85
1.07	10	0	-35	-70	45	70
1.08	25	10	-55	-55	80	65
1.09	45	70	-45	-30	90	100
1.10	45	25	-25	-20	70	45
1.11	45	65	-5	-15	50	80
1.12	55	60	-15	-25	70	85
1.13	45	50	-65	-85**	110	135
1.14	65	70	-20	-20	85	90
1.15	50	50	15	-30	35	80

Table 4.1: In vivo and predicted range of motion for all affected forearms. Positive value indicating pronation, negative supination.

*Positive value for the range of supination means that the patient can not reach a supination position and thus the closest pronation range to the neutral position is used.

**The central band showed no increase in length above 103% and thus the range of supination of the unaffected forearm is used as prediction.

	All cases (n=15)	Excluding patients without supination range (n=13)
Pronation	17.6	17.0
Supination	19.4	15.2
Full range	24.8	17.9

Table 4.2: Relative mean squared error (RMSE) for the prediction of pronation, supination and full range of motion of affected forearms.

effect is not seen in range for the unaffected forearms, while in malunited forearms this effect is seen for every patient. In supination the difference in MID is less significant. Only in the proximal and middle parts of the forearm the distances are significantly different. This could be because the central band attaches at the distal diaphysis of the ulna, influencing the distance. The location of the deformity can also have an influence on this distance, but this is not considered as a factor in this research.

At last, CBL is shorter in the affected forearms than in the unaffected forearms. This is true for pronation and supination. However, when looking at CBLR a relative increase is seen in pronation and supination, but this change is not significant. It does make clear that in malunited forearms the length changes significantly and this has an effect on restricting supination, but at the moment it is hard to set a threshold. Abe et al. does find the same for CBLR [1]: the length becomes shorter in pronation and larger in supination, but is not significant compared to unaffected forearms.

In this state the model can predict range of pronation, supination and the full arc with a certainty between 15 and 18 degrees for patients who can reach the neutral position. It is notable that the error for the full range is comparable with the error for the supination and pronation alone. This could point at a wrong neutral position for the forearms. If the maximum pronation is set on the position just before bone impingement occurs, this could lead to a better prediction. The central band increases in length during supination in all the malunited forearms, so it would still be possible to set a threshold on CBLR. This would probably only shift the prediction window. But this would neglect the position of the DRUJ completely and only look at the distance between the bones.

There is one other model that predicts range of motion in malunited forearms from the length of the central band, but this is a geometric model, which is not yet proven in vivo. [64] Yasutomi et al. connect their findings to angulation, but these findings are not in line with what we found in chapter 2. However, when we make that connection, we see that patient 1.13, who shows no difference in central band length during supination, has almost no angulation of the ulna in the radio-ulnar direction. Patient 1.07 shows an ulnar angulation of the ulna and shows a decrease in length of the central band in supination. These are the only patients with a different pattern for the central band. Following this logic, patient 1.06 should also show a shortening of the central band in supination, but this is not the case.

There are some limitations to this method. The first limitation concerns the determination of the neutral position and the use of this position in the prediction. The neutral position is needed to predict the range of motion and thus the forearms must be positioned in this way. The unaffected forearms are scanned in different positions, some in pronation and some in supination. To improve the modeling it would be better to make sure that the forearms are scanned in the neutral position. At the moment one CT-scan of a cadaveric arm is used to position unaffected arms to the neutral position and then the affected forearm is positioned into the neutral position using the unaffected forearm. This is not ideal, because if this scan is not rightly positioned an error is applied in every forearm. While modeling rotation in the neutral forearms does not lead to problems, the affected forearms show overlapping surface models in positions that should be reachable according to the in vivo measurements. This could be due to an error in the neutral position of the cadaveric scan, or the neutral position is altered in the malunited forearms. While literature does describe that the rotation axis of malunited distal radius fractures are not different than their unaffected forearms, there is no research for malunited diaphyseal fractures and the effect on the kinematics of the forearm [35]. Especially because these fractures occur in a young patient population, growth and remodeling of the bones could lead to a change in kinematics. The forearm could adapt to the new situation, which could lead to a different neutral position.

The other disadvantage of the use of the neutral position is that the range of motion for patients without a pronation or supination range can not be predicted. The central band is at the moment only restrictive relative to the length in neutral position. If this length is already too large, which is probably the case for patient 1.15, the relative value will not be right. This would require to look at the absolute values, which require to know the ratio between central band length and length of the forearm or to use more advanced models.

Second, the location of the central band is at the moment determined by the length of the radius and ulna using data from one cadaveric study. While the results do point at ligament contracture, the landmarks for the origin and insertion of the central band must be located more precise to draw conclusions. This is especially true for malunited forearms with internal angulations. MR scans or more advanced CT techniques can be used to determine the attachment landmarks [32, 19]. In the long term statistical shape modeling can be used. Furthermore, not only the length of the middle fibers is of interest for contracture, but the proximal and distal fibers are of separate interest as well because the central band becomes broader from origin to

insertion. This is because the central band has diagonal fibers and spreads out [30]. The change in length distally can be therefore larger than proximal. This could also depend on the location of the fracture, another factor which, like already said, must be considered in future research.

Finally, the status of the soft tissue is not taken into consideration. Not only there are more ligaments in the interosseous membrane of the forearm, but the muscles and capsules can have an influence on rotation as well. While some other ligaments can also be measured in this model by placing landmarks, muscles provide the rotation. They are effectors of movement rather than results. In conclusion, distance between the radius and ulna is different in a forearm after a malunion of the diaphysis, which could explain the rotational restriction that occurs. Enlargement of the space between the bones corresponds with the contracture of the central band, while reduction of the space leads to a situation close to bone impingement. Because both effects are dependent on bone size and thus the distances and lengths relative to the neutral position must be used, determining the neutral position of the forearm and the real attachment location of the central band are of importance before this model can be used to predict rotational limitation.

5

Clinical relevance and future research

This research proved that a loss of rotation after a malunited diaphyseal fracture of the forearm can be explained by measuring the central band length and checking for bone impingement. Minimal bone distance gives a good indication for what happens during rotation, but in supination the distance is not significantly different along the full diaphyses. Compared to the link between angulation of the bones and rotational limitation, which only gives an indication of the limitation based on the directional angulation of the ulna in two planes, the kinematic model can give an indication if bone impingement or contracture of the central band occurs and shows directly what the origin of the rotational restriction is. The error between 15 and 18 degrees however makes the prediction not clinical feasible at the moment.

The relevance of this information can be summarized in one question: does releasing the central band in patients with rotational restriction lead to an adequate improvement of rotational function without the need of performing a corrective osteotomy? In theory, there is a specific group of patients in which this could be a sufficient solution. These patients have a prominent supination loss because of enlargement of the central band. The loss of pronation must be less prominent, sufficient for daily tasks and no other symptoms such as pain or a large cosmetic difference between the arms must be present. Even then the question is if no other structure, ligament, muscle or skin, restricts further movement. Furthermore, the forearm can lose stability when the central band is cut and these effects must be considered as well.

Bone impingement can only be solved with a corrective osteotomy. So in short, the outcome of this research does not lead to an immediate change in how a diaphyseal malunion with rotational restriction is considered. But this research did give insight in how a larger bone distance is of importance for planning corrective osteotomies and the kinematic model used can be improved with in vivo landmarks for the central band and determining the neutral position. At the moment the greatest strength of the model is the automatic modeling of forearm rotation with patient specific anatomy as only input. Bone distance and bone overlapping are automatically calculated and visualized, which can improve the understanding for patients and surgeons. The validation showed small errors between the positions of the model and the cadaver arms, so while the model must be improved to be clinically usable, it does give a fast, automatic and rough idea how the malunion restricts rotation.

There are still some differences however between the model and reality. First the rotation of the radius relative to measured rotational position (pronation or supination) is unambiguous. Chapter 3 showed that the angle of rotation applied to the radius to rotate from neutral position to a rotated position is not equal to the measured position in pronation and even less in supination. It could be that this is different in each person and that there is also possible some translation and tilt in the dorsovolar direction as is described by Akhbari et al. [2]. Second is determining the neutral position. This position is important for relative distances. While the best solution is to ensure that the scans are made in the neutral position if this is possible, malunited forearms can show a different or altered neutral position due to growth of the forearms, but this is unknown. The internal angulation of the radius and ulna could be describing this change, but to conclude this it must be known what the position is of the forearm in terms of pronation and supination during the scan to link this data. To really validate the model, scans of malunited forearms must be made as well in different positions to make sure that not only unaffected forearms are modeled correctly and that the kinematics of forearm rotation are not strongly altered after a malunion of the diaphysis. Even better would be to scan the DRUJ dynamically to really understand what happens in vivo during rotation. At last, the location of the deformity

was in no part of this research considered. Abe et al. points out that a deformation in the distal third of the diaphysis leads to a different effect than a proximal or middle third deformation [1]. Location must therefore be considered not only in the angular measurements, but also for the bone distance in supination because it adds a factor where you expect the largest increase in distance.

A

Individual patient data

Pt.	Aff. side	Deformity Radius						Ulna						Range of motion					
		DVA	RUA	IA	TA	DVA	RUA	IA	TA	Unaffected side	Affected side								
1.01	R	14.9	2.0	1.5	15.0	-2.7	9.4	-14.2	9.8	65	80	145	45	20	60				
1.02	R	19.8	11.0	34.6	22.7	2.6	17.9	5.2	18.1	65	90	155	30	20	50				
1.03	L	16.1	0.9	27.2	16.1	-6.6	12.6	12.6	14.2	70	75	145	65	5	65				
1.04	L	19.0	-1.2	-20.4	19.0	-20.1	1.8	22.5	20.2	65	80	145	55	-5	50				
1.05	L	19.5	-3.2	7.4	19.8	-1.6	13.9	3.4	14.0	75	85	160	60	10	70				
1.06	L	21.9	10.8	-22.0	24.4	-15.8	-7.5	3.9	17.5	65	90	155	25	65	90				
1.07	L	3.1	-12.8	-4.2	13.2	20.9	-13.3	3.8	24.8	75	85	160	5	35	40				
1.08	L	14.8	14.1	49.4	10.4	5.6	11.8	-2.7	13.1	75	80	155	25	55	80				
1.09	L	15.0	-3.9	0.1	15.5	-3.5	10.4	4.3	11.0	65	90	155	45	45	90				
1.10	L	25.3	12.9	-3.1	28.4	-14.0	6.8	14.7	15.6	70	100	170	45	25	70				
1.11	R	20.9	8.8	9.4	22.7	-14.4	8.2	-3.4	16.6	80	90	170	45	5	50				
1.12	L	7.1	-2.4	29.7	7.5	-1.9	7.8	-0.8	8.0	60	85	145	55	15	70				
1.13	R	8.3	6.4	9.5	10.5	3.2	-0.5	-24.2	3.2	80	85	165	45	65	110				
1.14	R	8.0	-4.9	-2.8	9.4	3.8	16.2	0.9	16.6	65	85	150	65	20	85				
1.15	R	9.7	-5.7	4.2	11.3	7.1	5.0	7.9	8.7	60	85	145	50	-15	35				

Table A.1: Individual patient data used in this research. Aff. side: affected side, DVA: dorsovolar angulation, RUA: radioulnar angulation, IA: internal angulation, TA: total angulation. Positive values for DVA, RUA, IA are directed into the dorsal, radial and pronation direction respectively. The range of motion is rounded to fives to compare with the model.

B

Validation data

At the next page all the errors between the model and specimen scans are presented for all scanned positions. Abbreviations used are DV: dorsal (+) volar (-); RU: radial (+) ulnar (-); PS: pronation (+) supination (-). The applied angles are negative in pronation and positive in supination because it were right forearms.

Specimen 1	30 degrees supination			60 degrees supination			90 degrees supination		
Rotation angle (degrees)	41			70			87		
Coordinates (mm)	DV	RU	PS	DV	RU	PS	DV	RU	PS
Rotation axis (true)	0.10	-0.09	0.99	0.10	-0.09	0.99	0.10	-0.09	0.99
Rotation axis (model)	0.09	-0.07	0.99	0.09	-0.07	0.99	0.10	-0.07	0.99
Euler angles (true)	2.65	-4.50	40.17	2.06	-8.48*	69.18	1.04	-10.32*	86.60
Euler angles (model)	2.46	-3.80	40.68	2.55	-7.25*	69.46	1.84	-9.23*	86.44
Center of rotation (true)	0.26	6.75	0.55	-2.54	10.51	1.10	-4.57	12.26	1.76
Center of rotation (model)	0.06	7.29	0.49	-2.84	11.20	1.04	-5.34	12.66	1.41

Table B.1: True and modeled rotation axis, applied euler angles and center of rotation of supination of specimen 1.

* Difference larger than 1 millimeter or 1 degree between true and model.

Specimen 1	30 degrees pronation			60 degrees pronation			90 degrees pronation		
Rotation angle (degrees)	-36			-42			-48		
Coordinates (mm)	DV	RU	PS	DV	RU	PS	DV	RU	PS
Rotation axis (true)	0.09	-0.08	0.99	0.09	-0.07	0.99	0.09	-0.07	0.99
Rotation axis (model)	0.08	-0.07	0.99	0.09	-0.07	0.99	0.09	-0.07	0.99
Euler angles (true)	-4.05	1.52	-36.24	-4.53	1.33	-42.10	-4.96	1.19	-47.78
Euler angles (model)	-3.62	1.41	-35.84	-4.28	1.41	-41.82	-4.94	1.34	-47.80
Center of rotation (true)	-3.69	-5.05	-0.16	-4.28	-5.26	0.09	-5.04	-5.35	-0.05
Center of rotation (model)	-4.26	-5.16	0.00	-5.25	-5.73	0.05	-6.28	-6.21	0.11

Table B.2: True and modeled rotation axis, applied Euler angles and center of rotation of pronation of specimen 1.

* Difference larger than 1 millimeter or 1 degree between true and model.

Specimen 4	30 degrees supination			60 degrees supination			90 degrees supination		
Rotation angle (degrees)	14			37			76		
Coordinates (mm)	DV	RU	PS	DV	RU	PS	DV	RU	PS
Rotation axis (true)	0.08	-0.08	0.99	0.08	-0.07	0.99	0.08	-0.07	0.99
Rotation axis (model)	0.08	-0.06	1.00	0.08	-0.07	0.99	0.09	-0.07	0.99
Euler angles (true)	0.95	-1.20	13.64	2.10	-3.26	37.15	1.67	-7.60	75.85
Euler angles (model)	0.93	-1.02	13.92	2.01	-3.21	36.76	1.92	-7.56	75.53
Center of rotation (true)	0.66	2.34	0.26	1.05	6.13	0.67	-1.46	11.91	0.91
Center of rotation (model)	0.77	2.36	0.09	0.82	5.99	0.33	-2.23	10.95	0.94

Table B.3: True and modeled rotation axis, applied Euler angles and center of rotation of supination of specimen 4.

* Difference larger than 1 millimeter or 1 degree between true and model.

Specimen 4	30 degrees pronation			60 degrees pronation			90 degrees pronation		
Rotation angle (degrees)	-37			-48			-66		
Coordinates (mm)	DV	RU	PS	DV	RU	PS	DV	RU	PS
Rotation axis (true)	0.08	-0.06	1.00	0.08	-0.06	1.00	0.07	-0.06	1.00
Rotation axis (model)	0.07	-0.07	1.00	0.07	-0.07	1.00	0.07	-0.07	1.00
Euler angles (true)	-3.61	1.28	-39.33	-4.36	1.14	-47.81	-5.98	0.81	-65.92
Euler angles (model)	-3.26	1.53	-38.88	-4.10	1.56	-47.87	-5.73	1.19	-65.83
Center of rotation (true)	-4.98	-4.64	-0.34	-6.33	-4.97	-0.20	-9.41	-5.49	0.06
Center of rotation (model)	-5.00	-5.11	0.00	-6.58	-5.77	0.06	-9.91	-6.38	0.24

Table B.4: True and modeled rotation axis, applied Euler angles and center of rotation of supination of specimen 4.

* Difference larger than 1 millimeter or 1 degree between true and model.

C

Distance graphs

On the next pages the mean, minimum and maximum relative minimum interosseous distance (MIDR) and relative central band length (CBLR) are presented in graphs for the affected and unaffected forearms of all fifteen patients. The legend of these graphs is presented here once to save space.

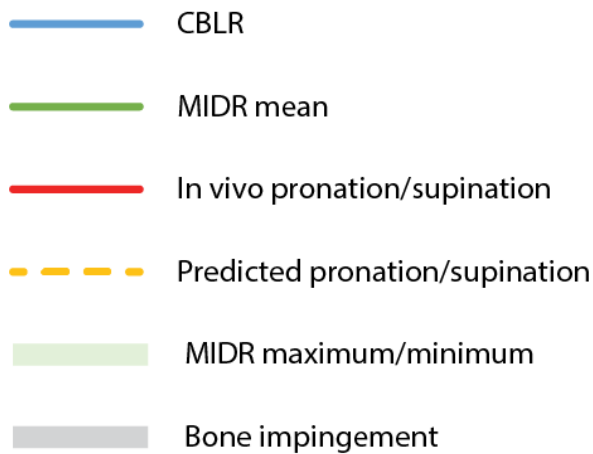


Figure C.1: Legend for the distance graphs as mentioned in chapter 4

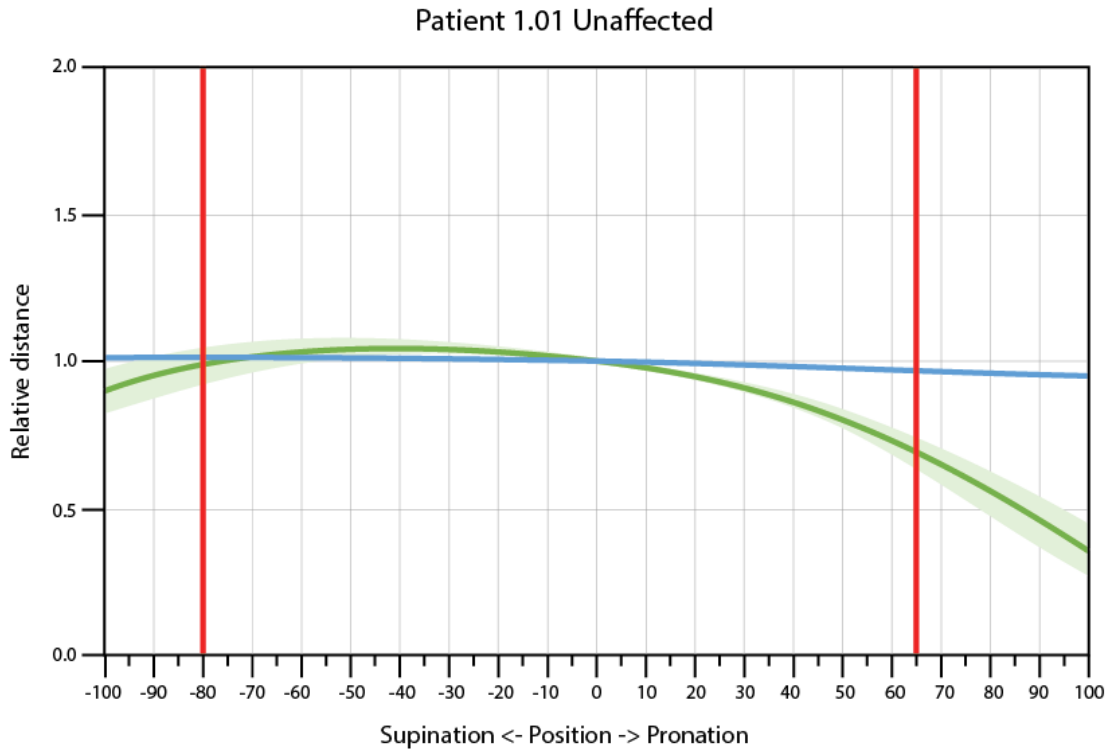


Figure C.2: Model outcomes for patient 1.01 unaffected forearm

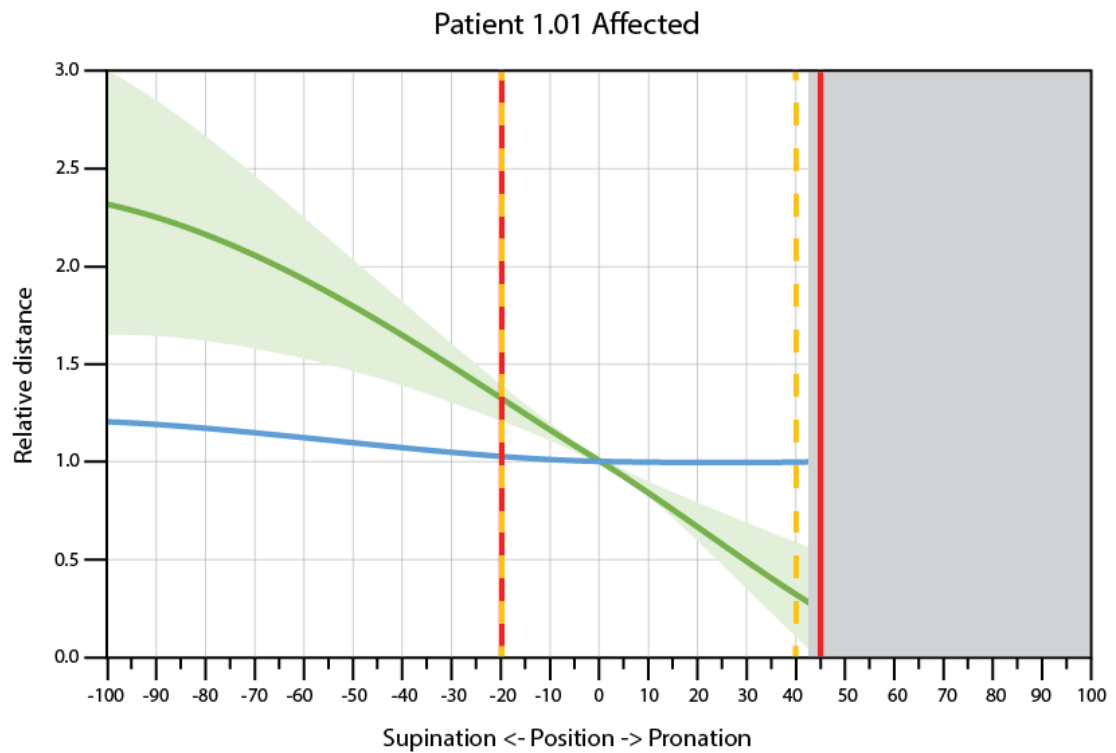


Figure C.3: Model outcomes for patient 1.01 affected forearm

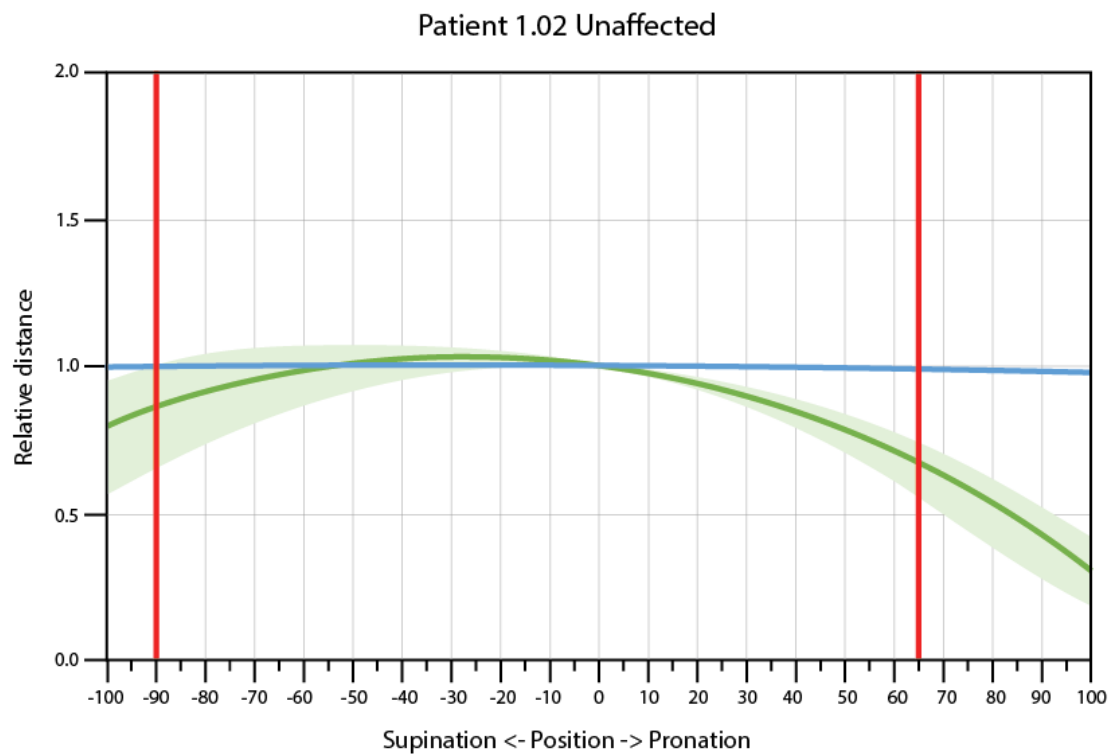


Figure C.4: Model outcomes for patient 1.02 unaffected forearm

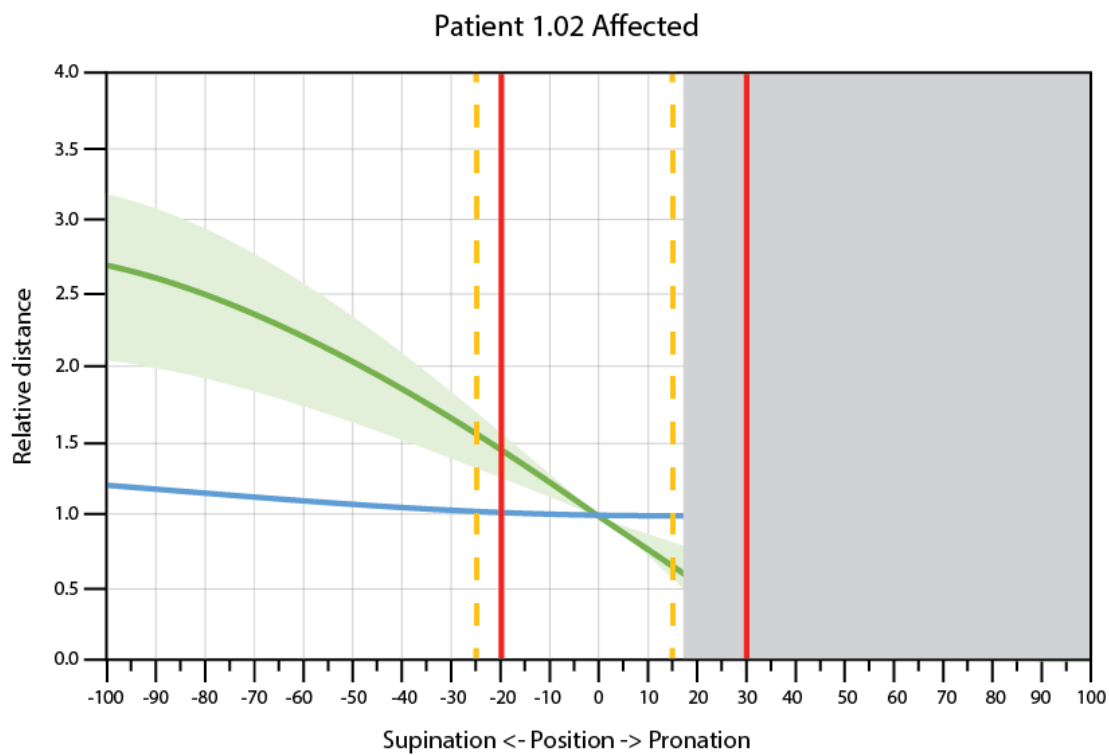


Figure C.5: Model outcomes for patient 1.02 affected forearm

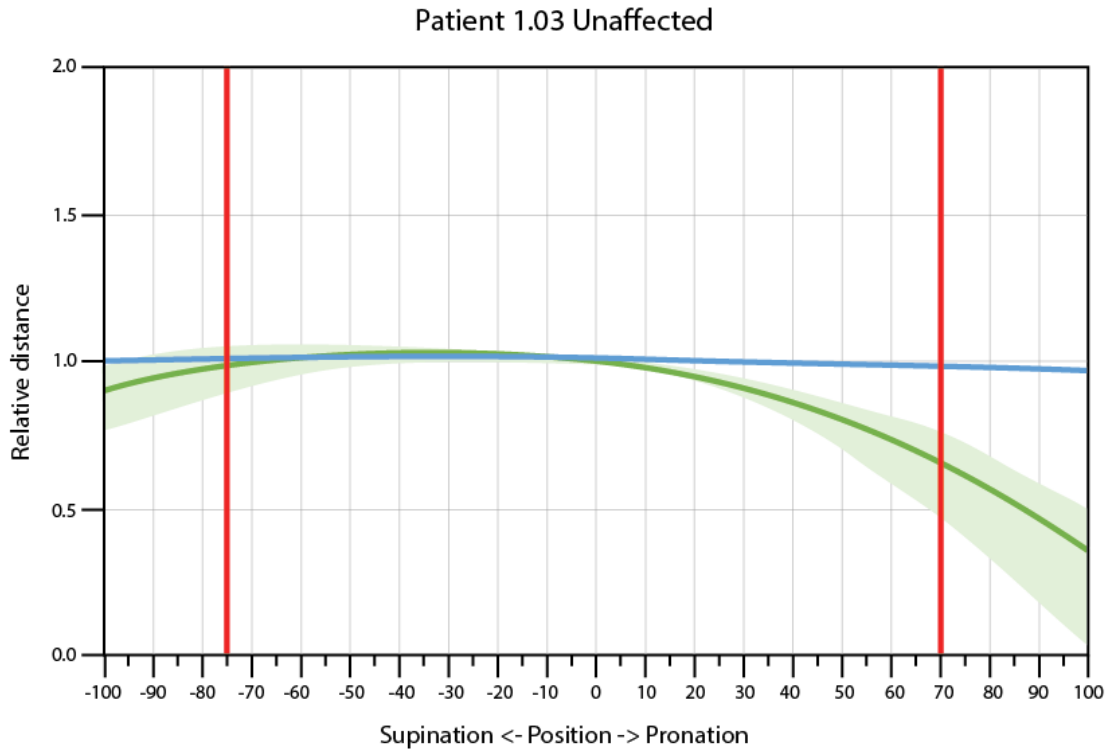


Figure C.6: Model outcomes for patient 1.03 unaffected forearm

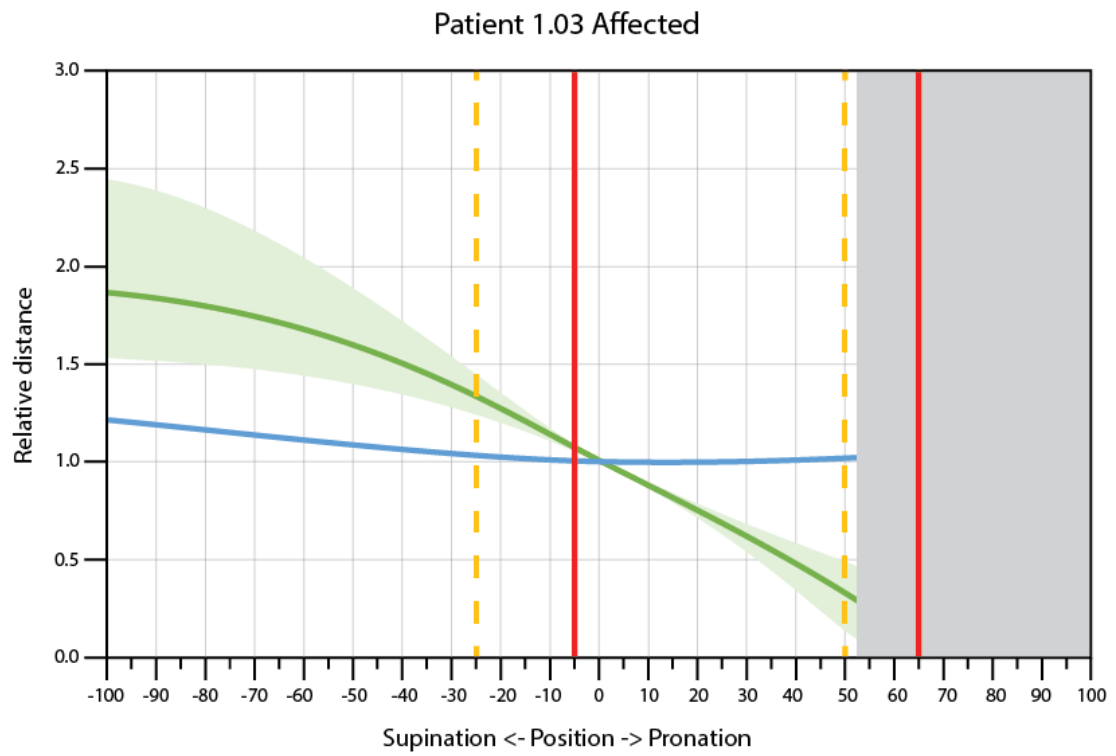


Figure C.7: Model outcomes for patient 1.03 affected forearm

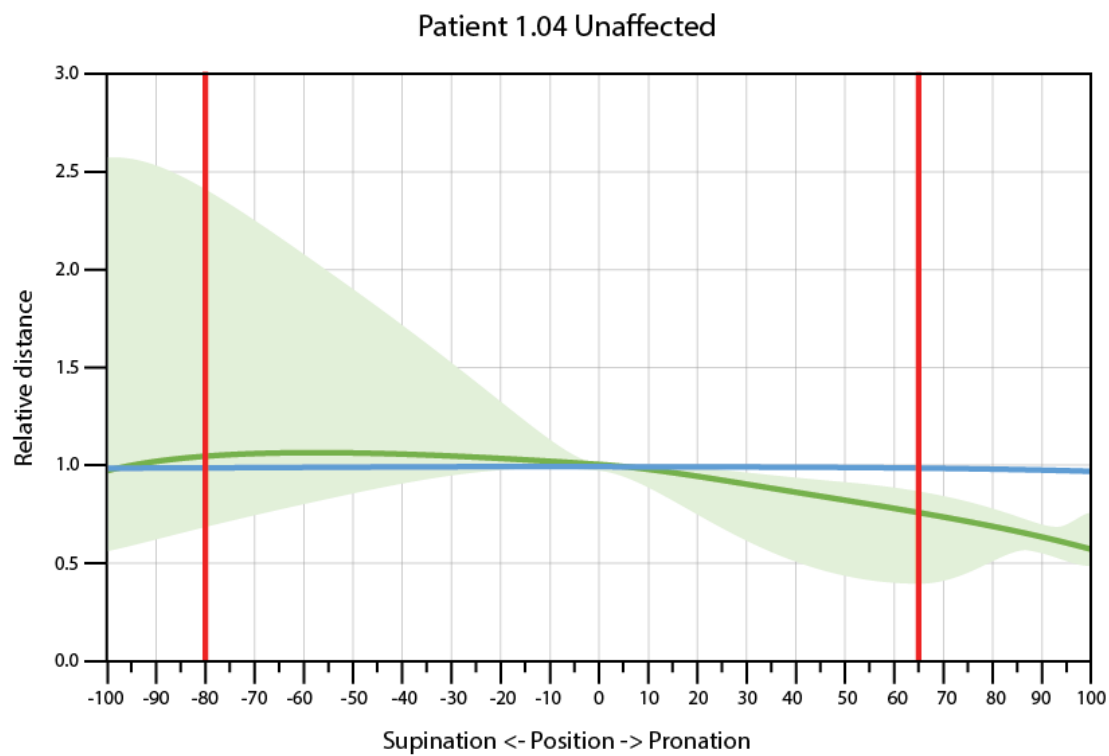


Figure C.8: Model outcomes for patient 1.04 unaffected forearm

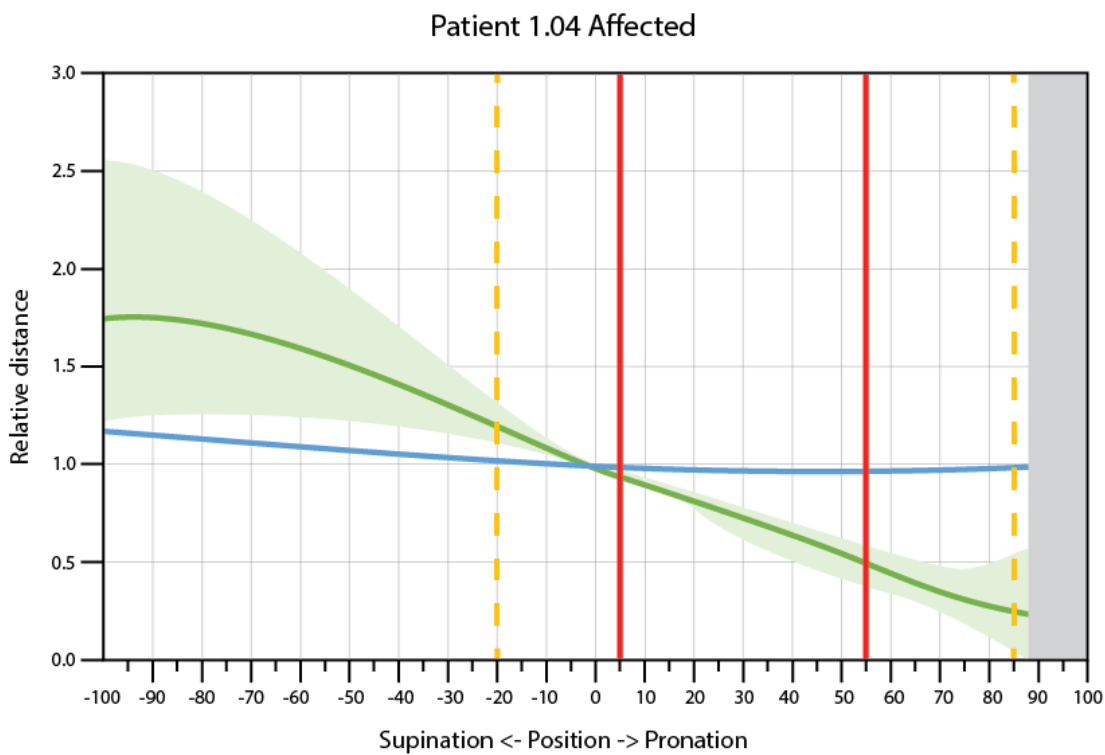


Figure C.9: Model outcomes for patient 1.04 affected forearm

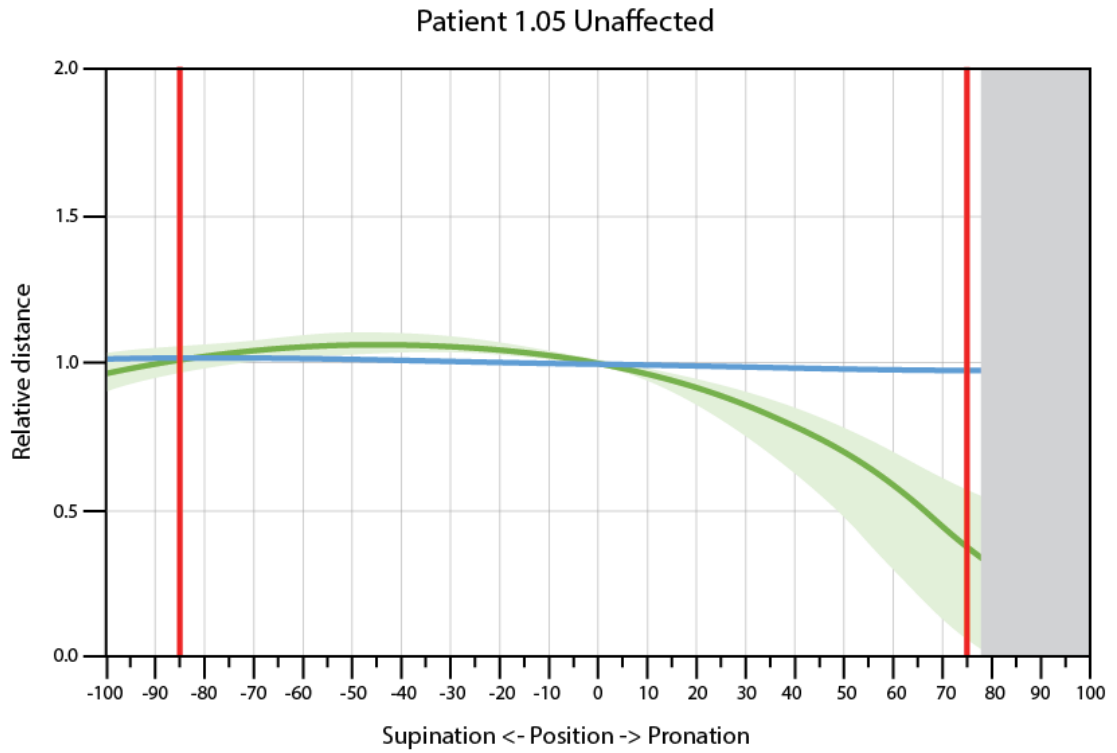


Figure C.10: Model outcomes for patient 1.05 unaffected forearm

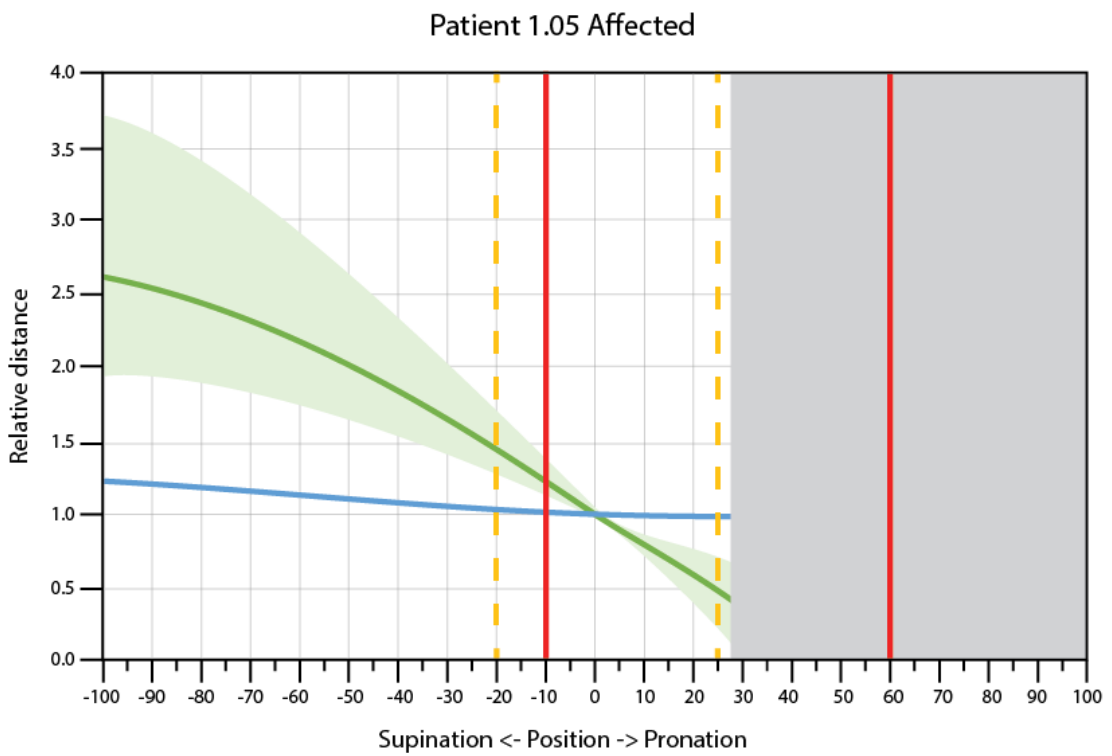


Figure C.11: Model outcomes for patient 1.05 affected forearm

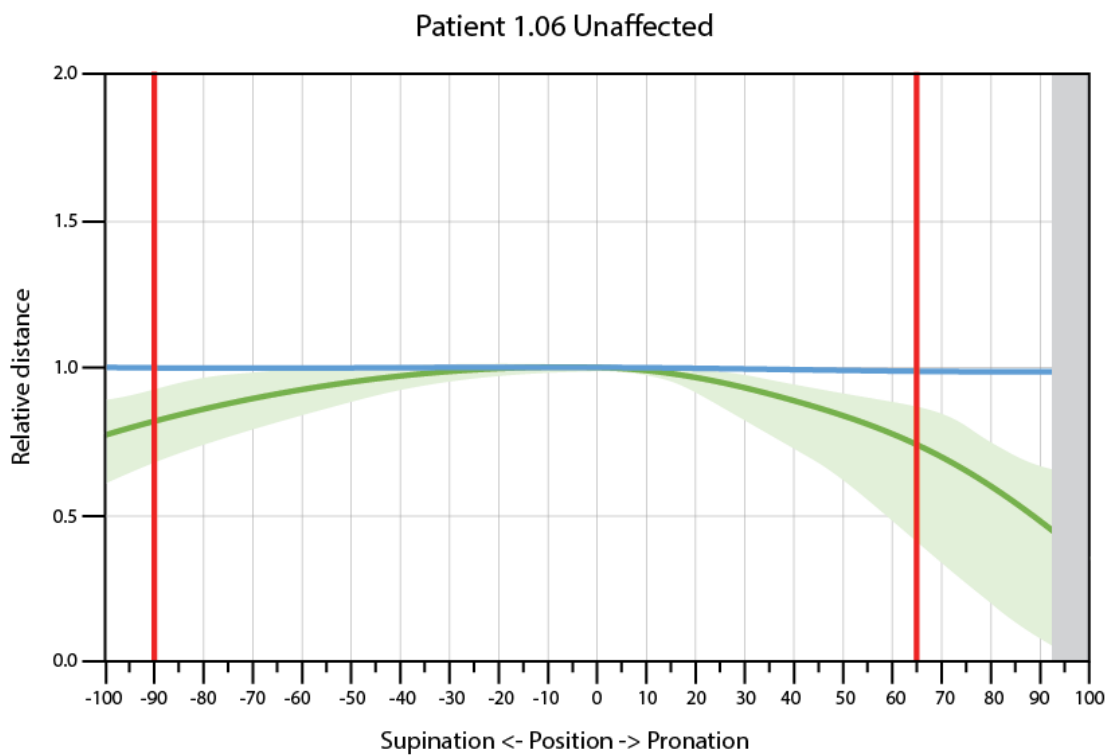


Figure C.12: Model outcomes for patient 1.06 unaffected forearm

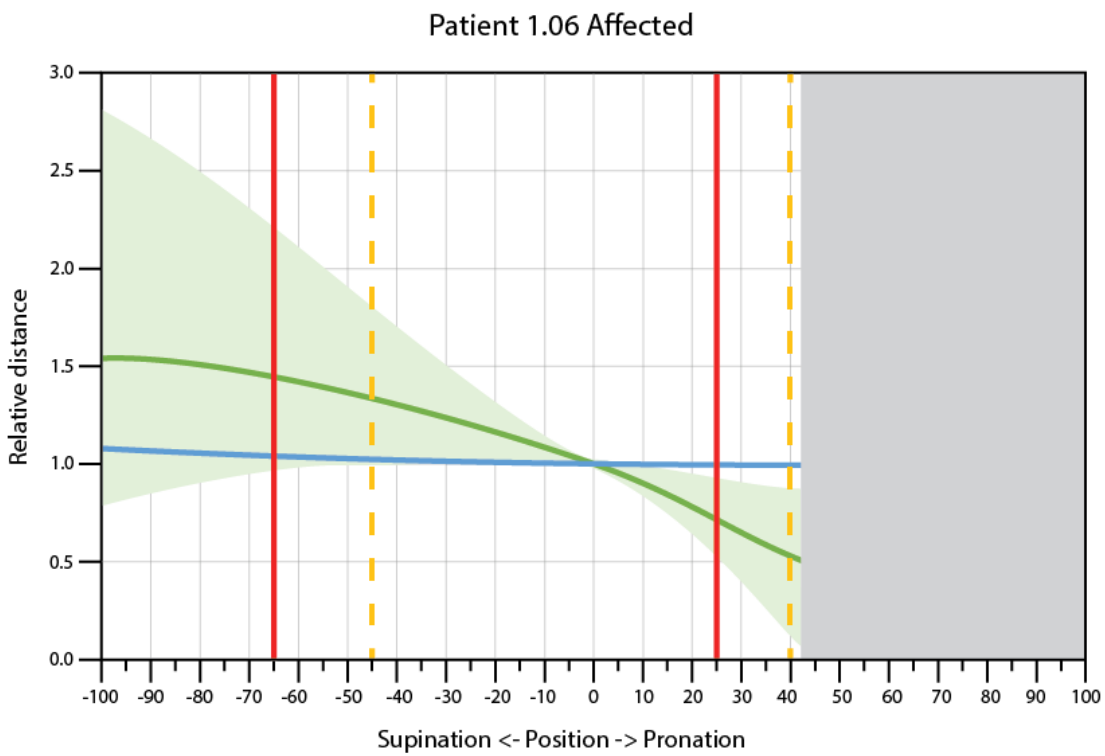


Figure C.13: Model outcomes for patient 1.06 affected forearm

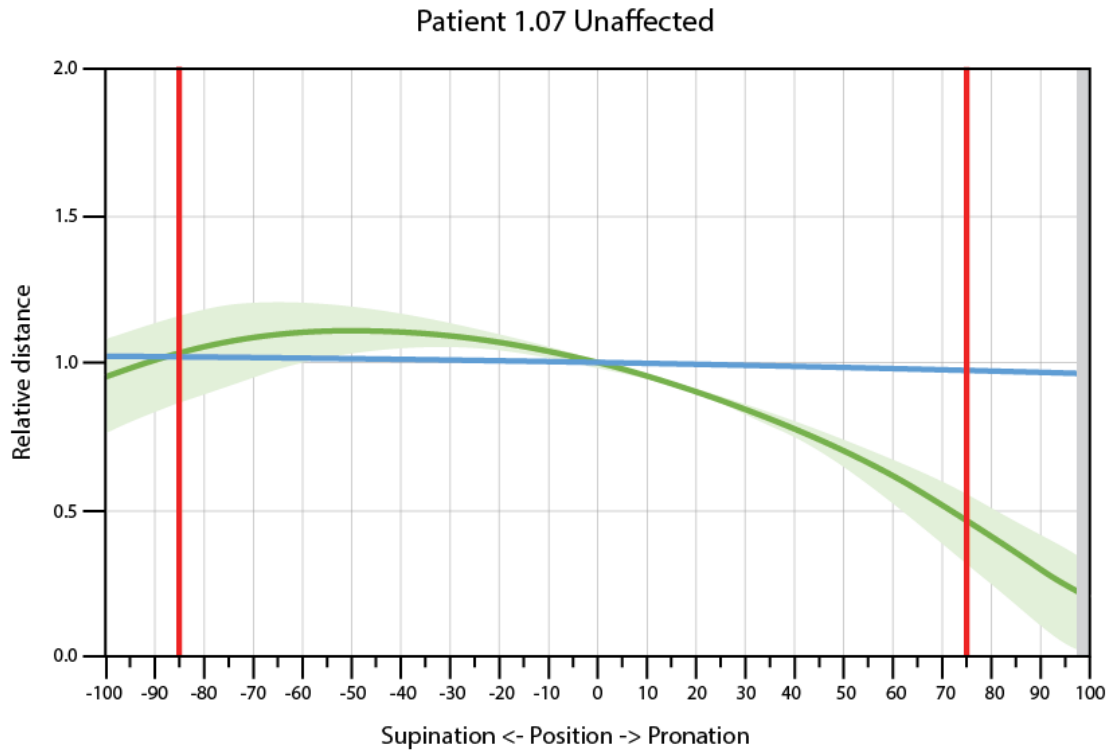


Figure C.14: Model outcomes for patient 1.07 unaffected forearm

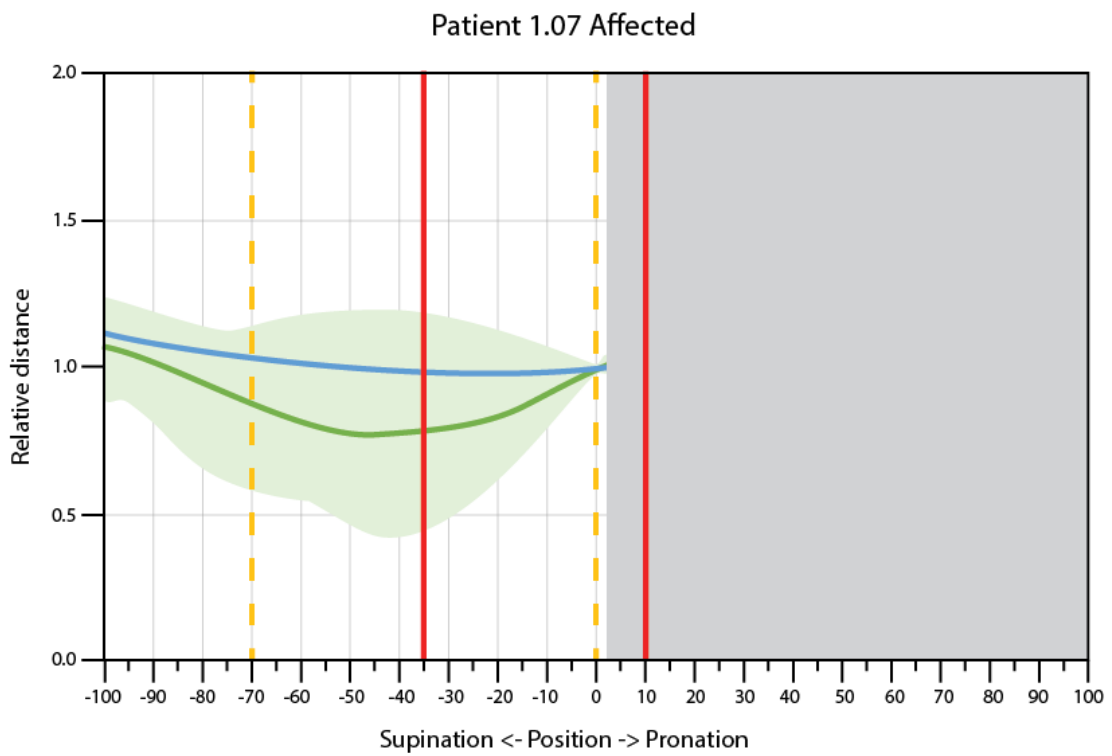


Figure C.15: Model outcomes for patient 1.07 affected forearm

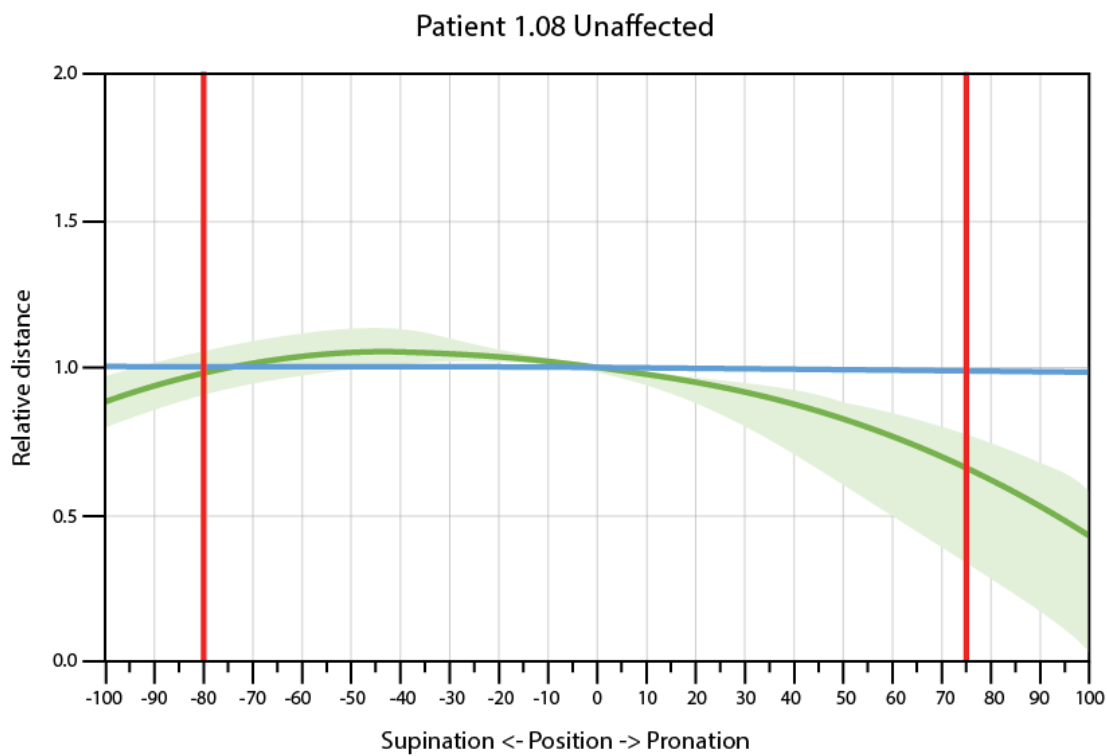


Figure C.16: Model outcomes for patient 1.08 unaffected forearm

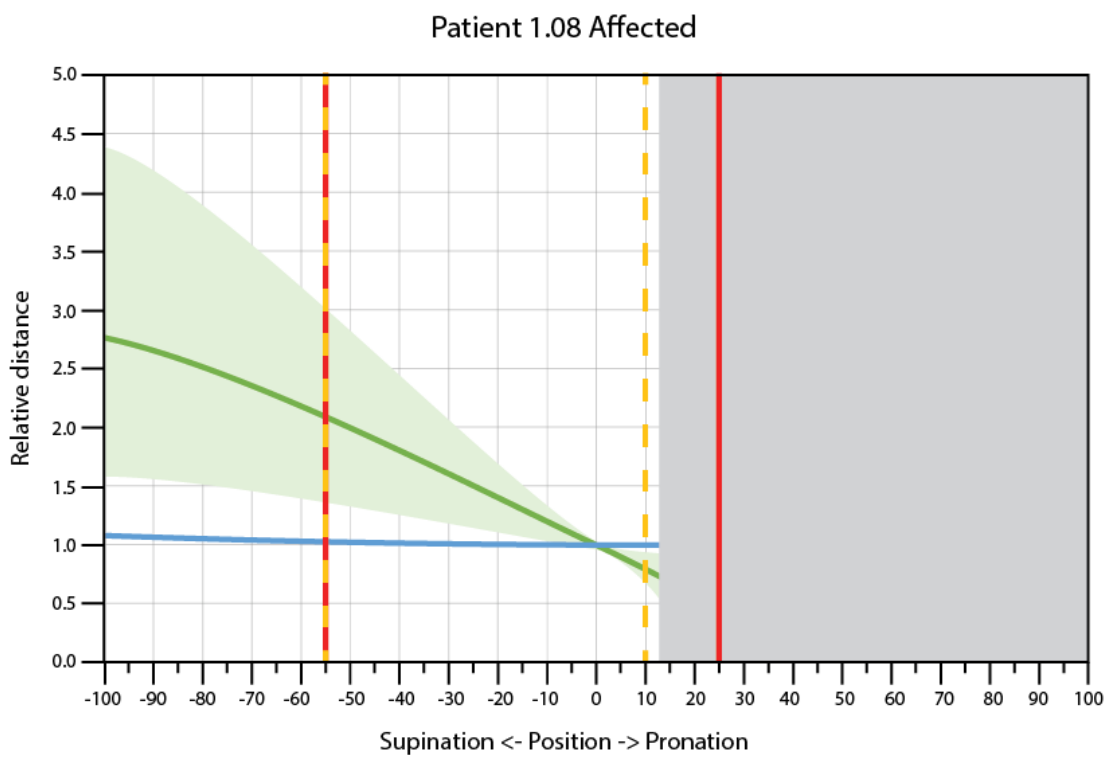


Figure C.17: Model outcomes for patient 1.08 affected forearm

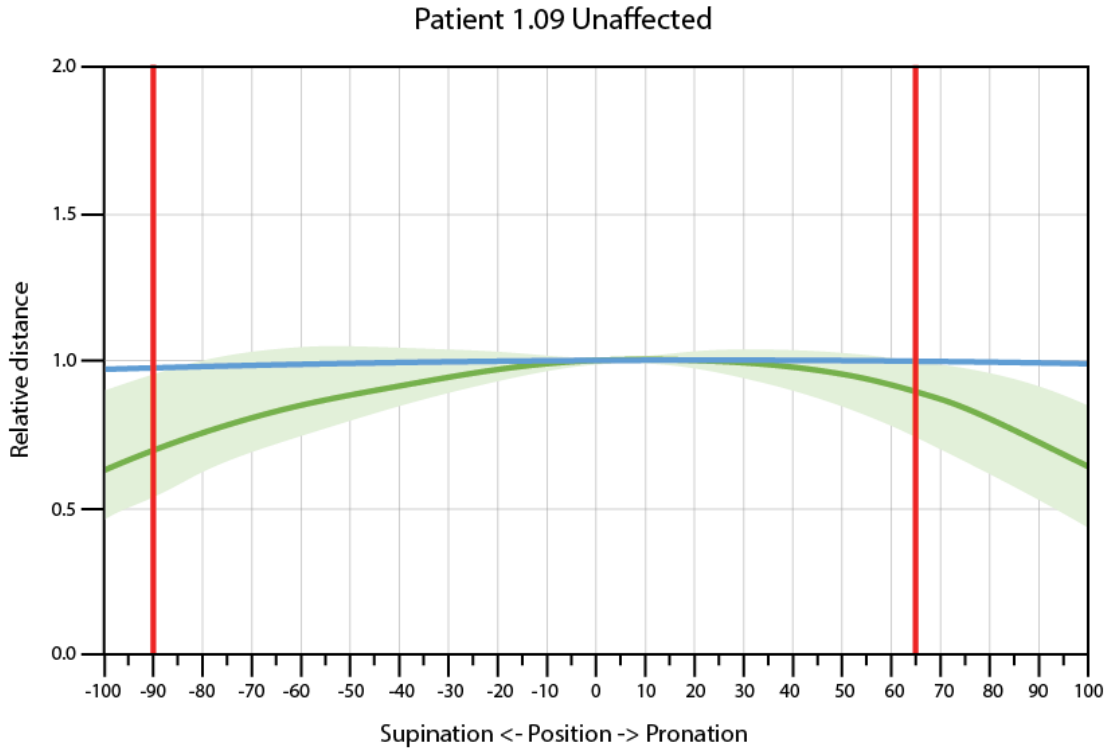


Figure C.18: Model outcomes for patient 1.09 unaffected forearm

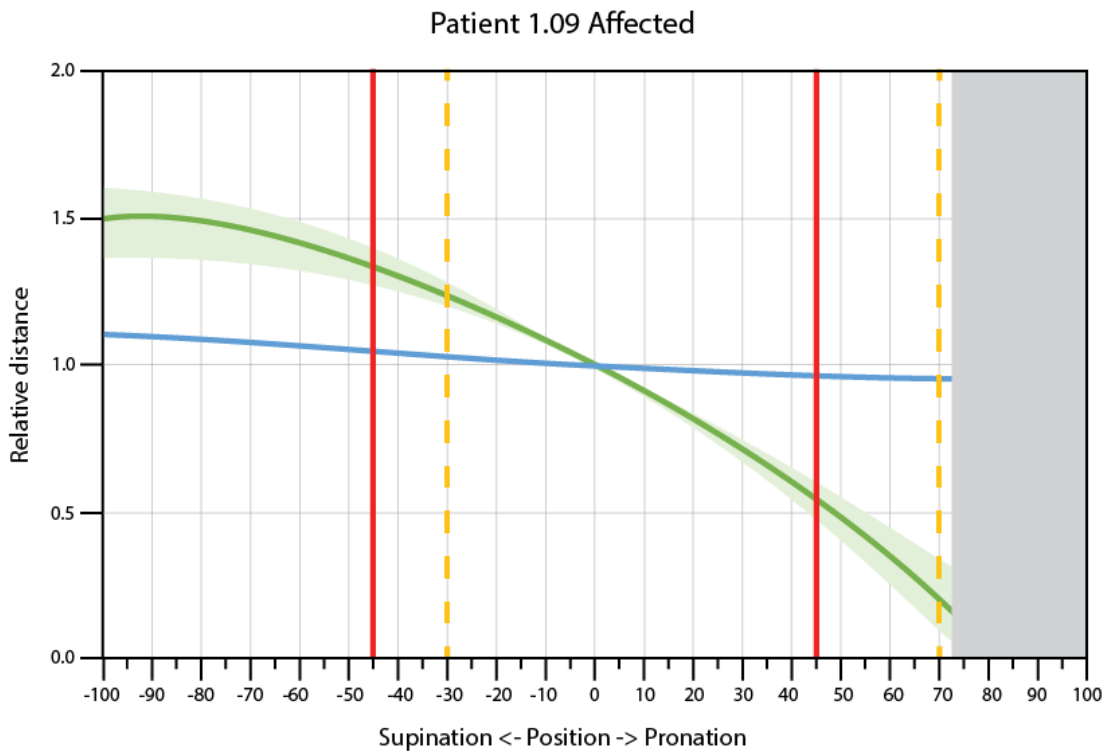


Figure C.19: Model outcomes for patient 1.09 affected forearm

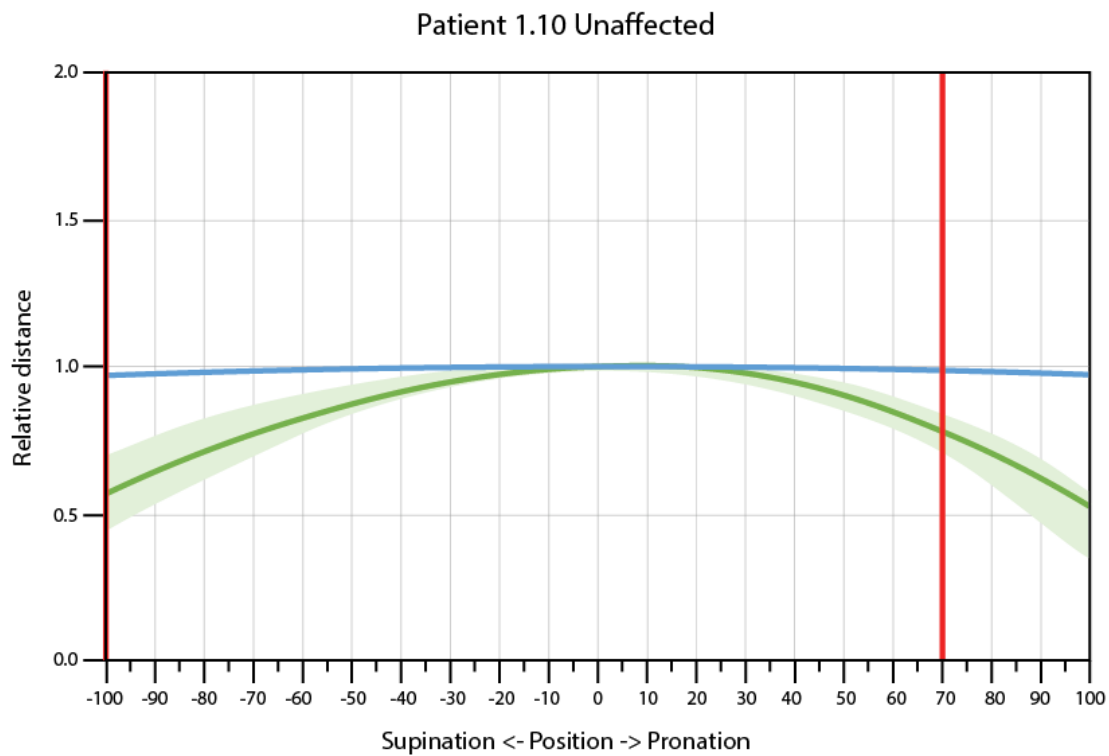


Figure C.20: Model outcomes for patient 1.10 unaffected forearm

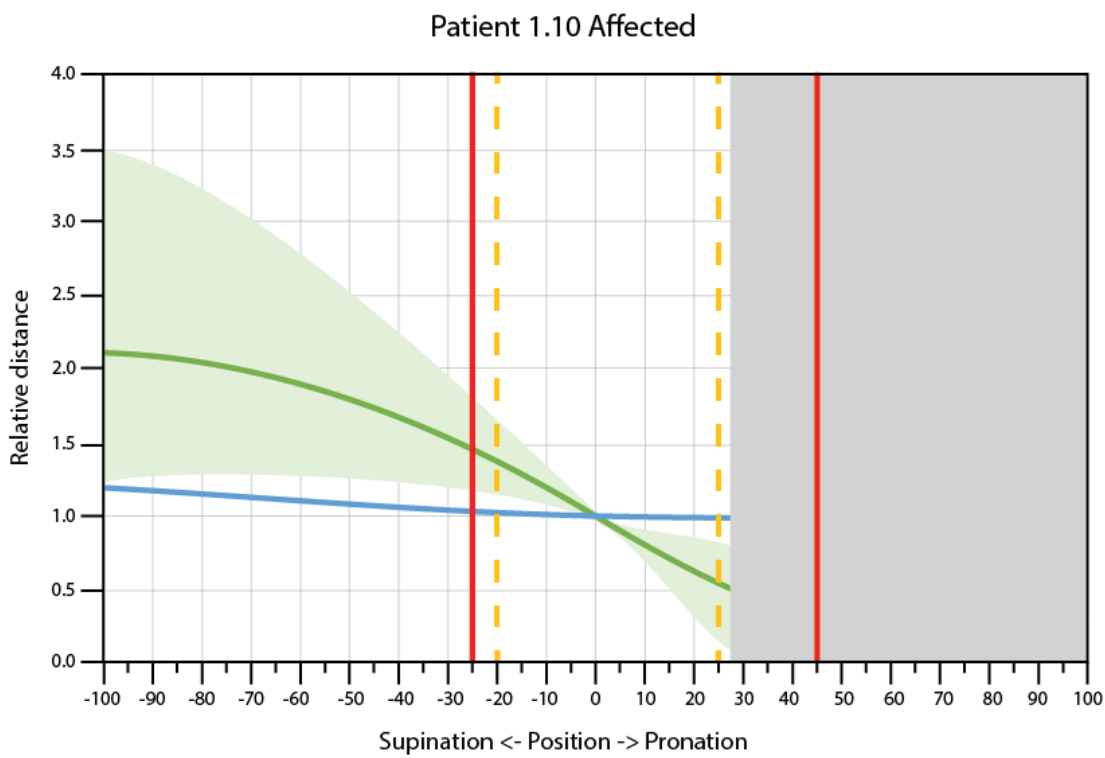


Figure C.21: Model outcomes for patient 1.10 affected forearm

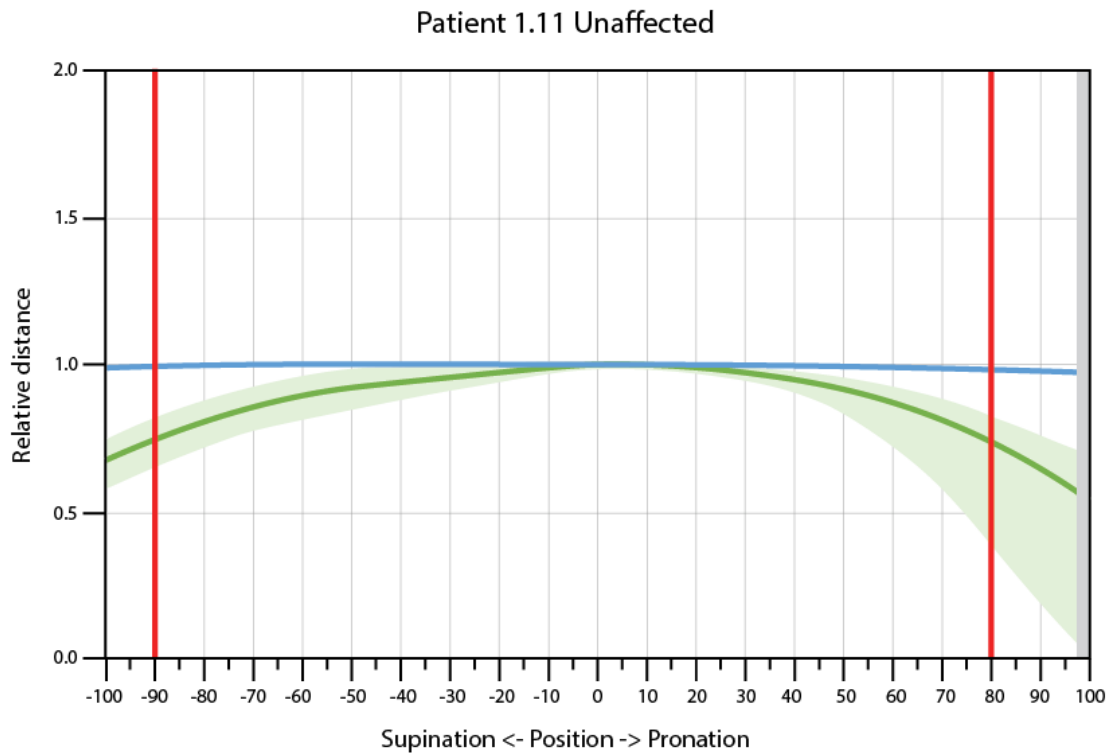


Figure C.22: Model outcomes for patient 1.11 unaffected forearm

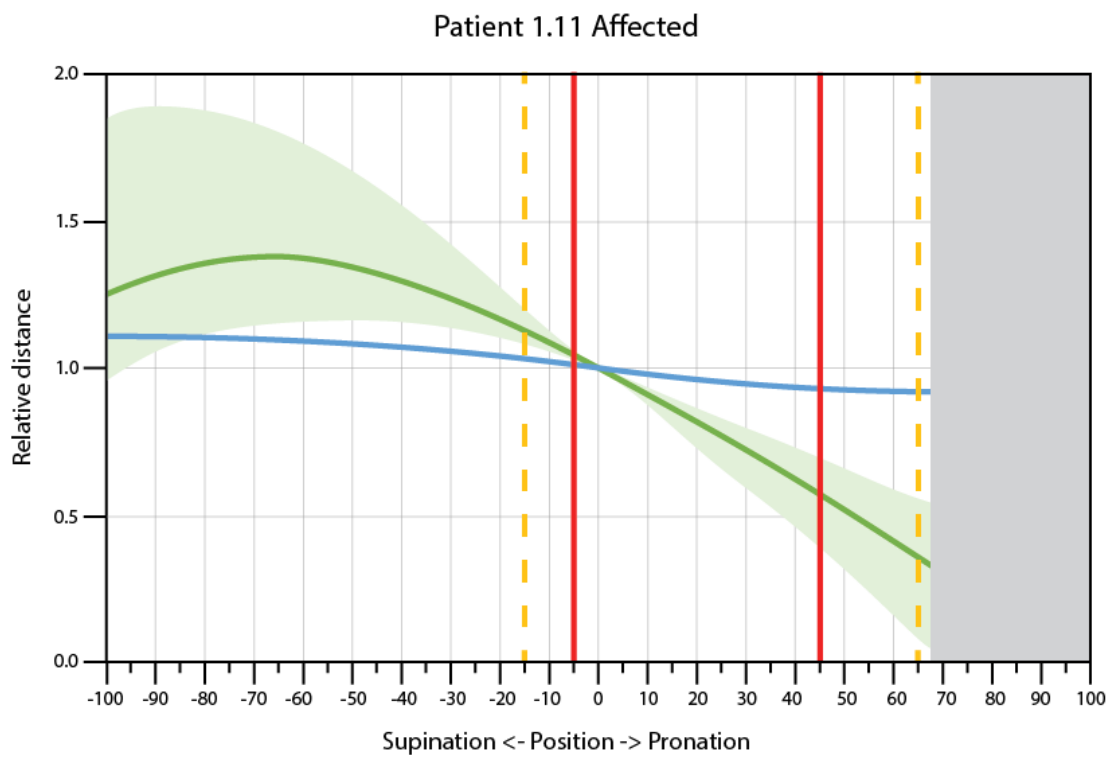


Figure C.23: Model outcomes for patient 1.11 affected forearm

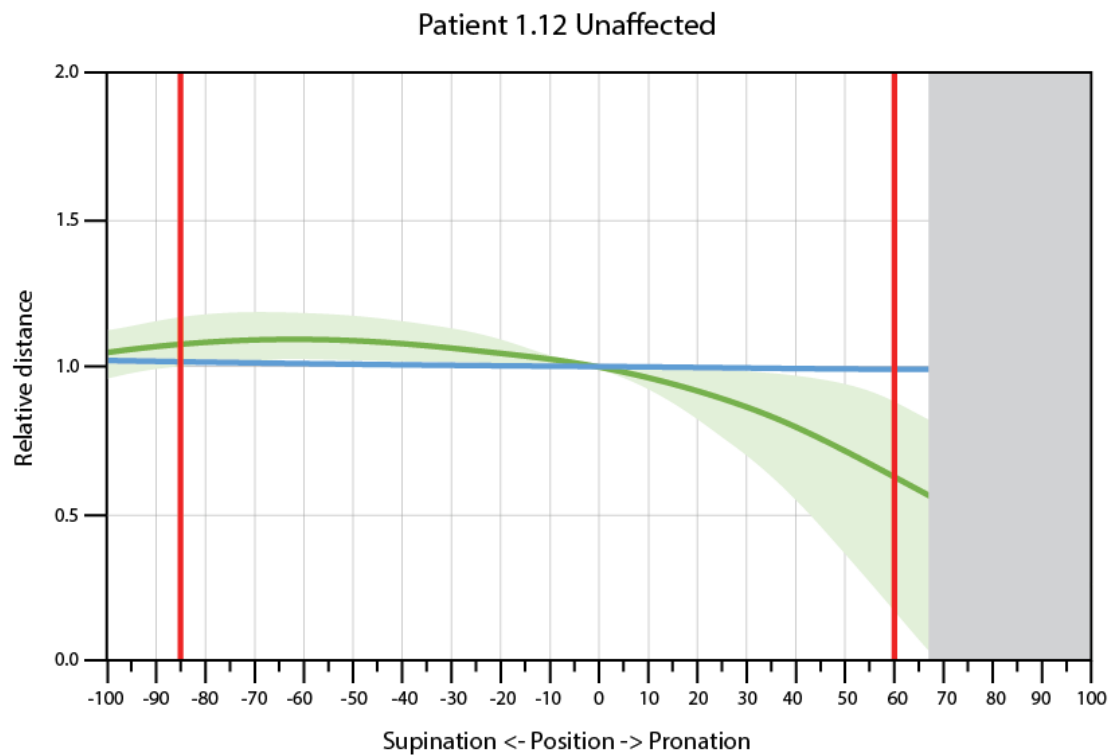


Figure C.24: Model outcomes for patient 1.12 unaffected forearm

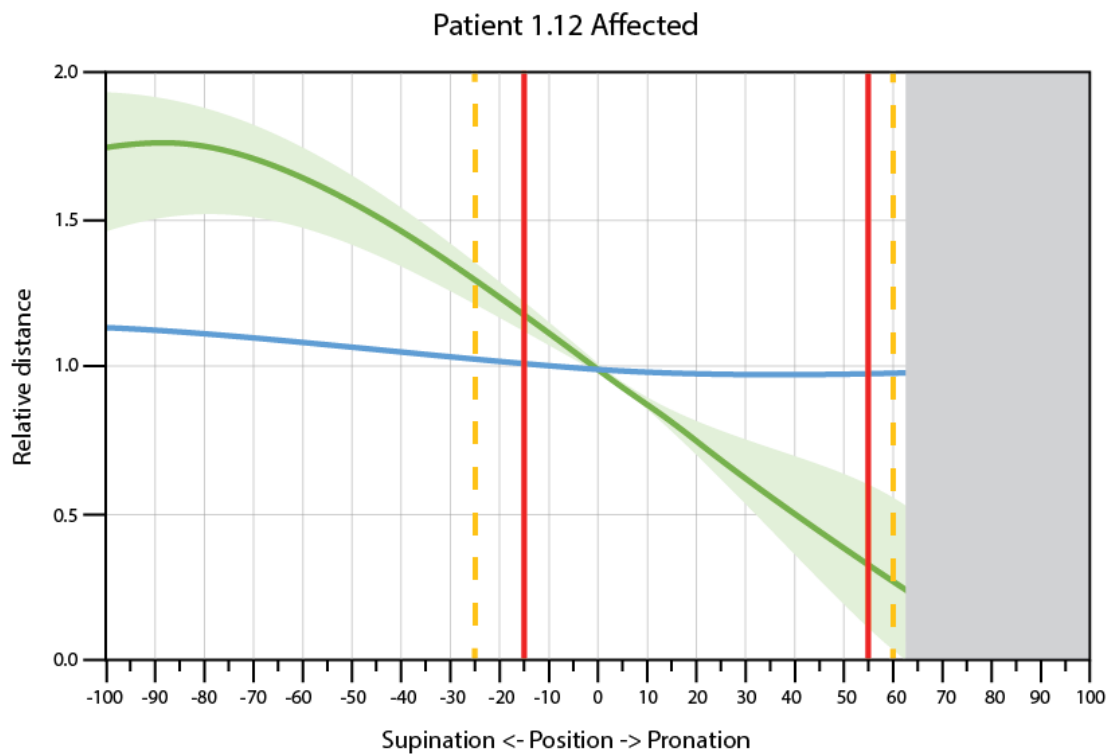


Figure C.25: Model outcomes for patient 1.12 affected forearm

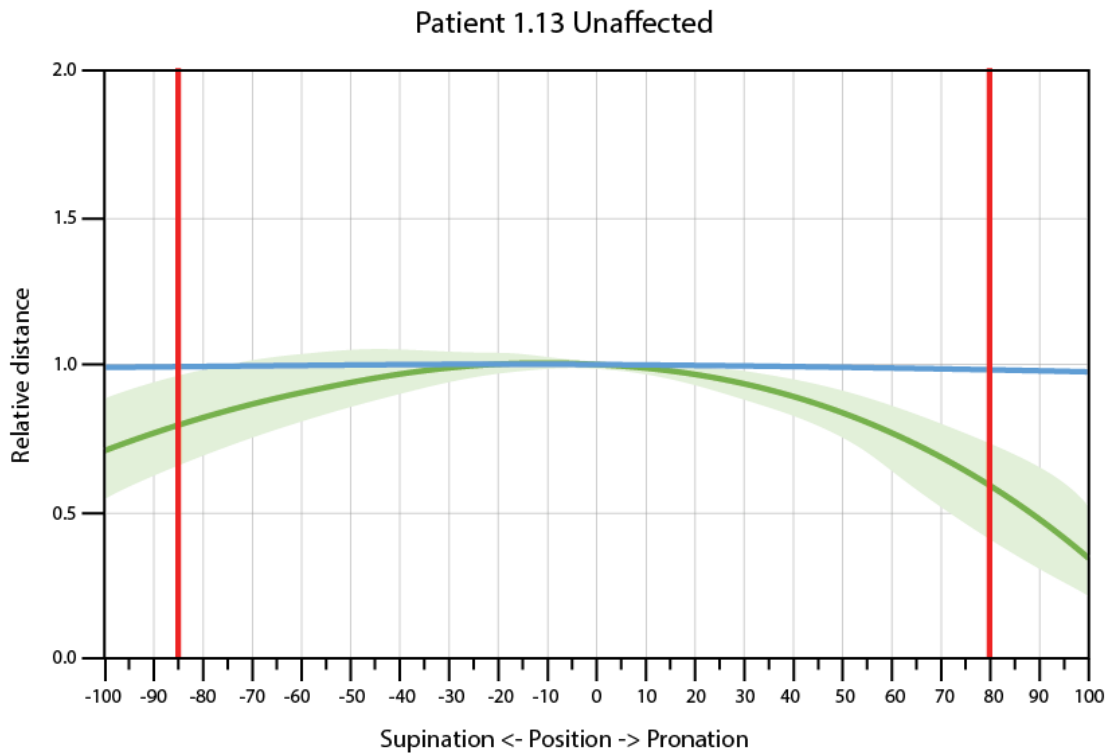


Figure C.26: Model outcomes for patient 1.13 unaffected forearm

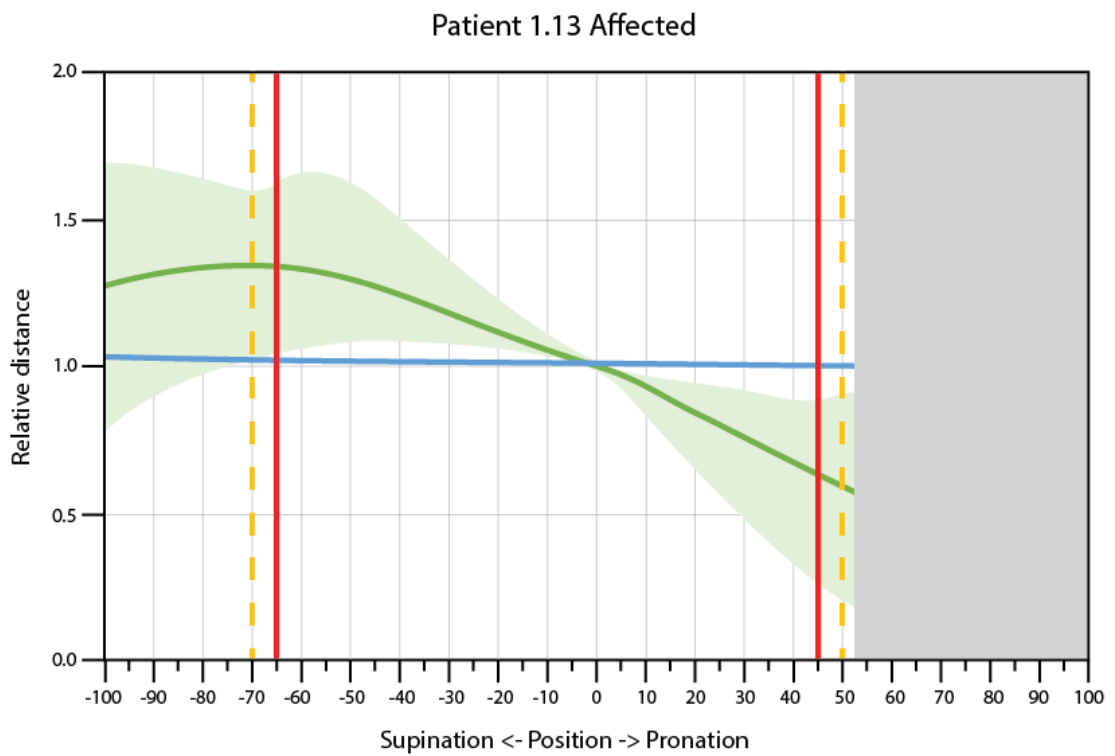


Figure C.27: Model outcomes for patient 1.13 affected forearm

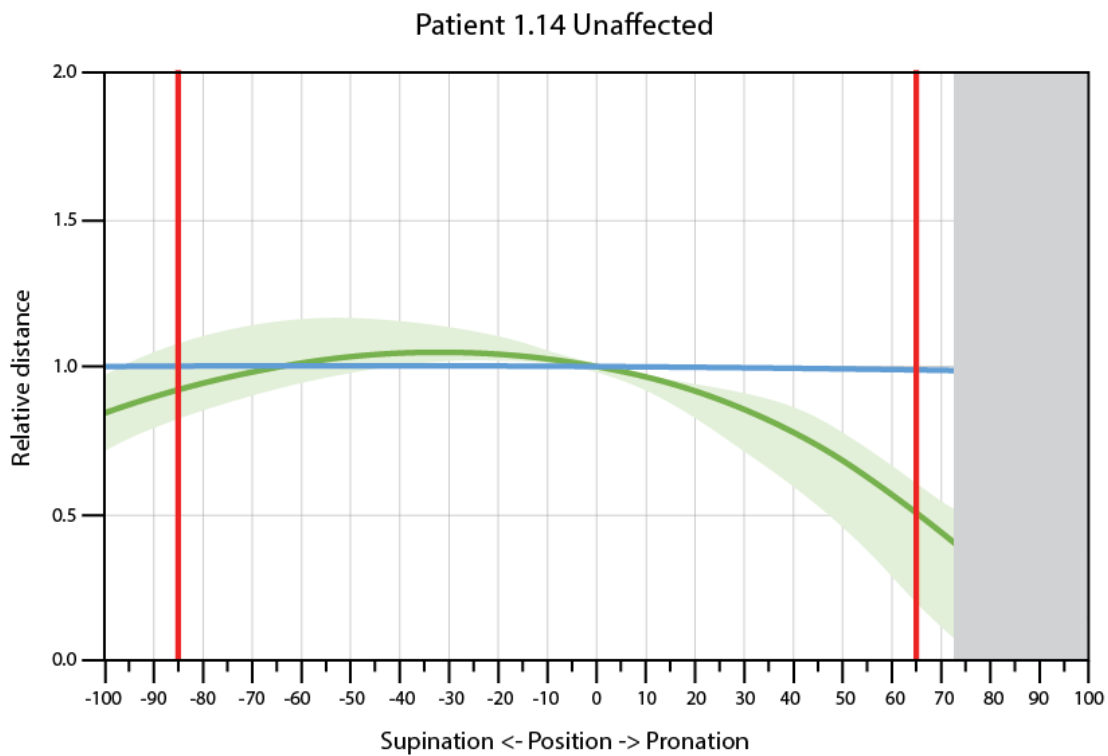


Figure C.28: Model outcomes for patient 1.14 unaffected forearm

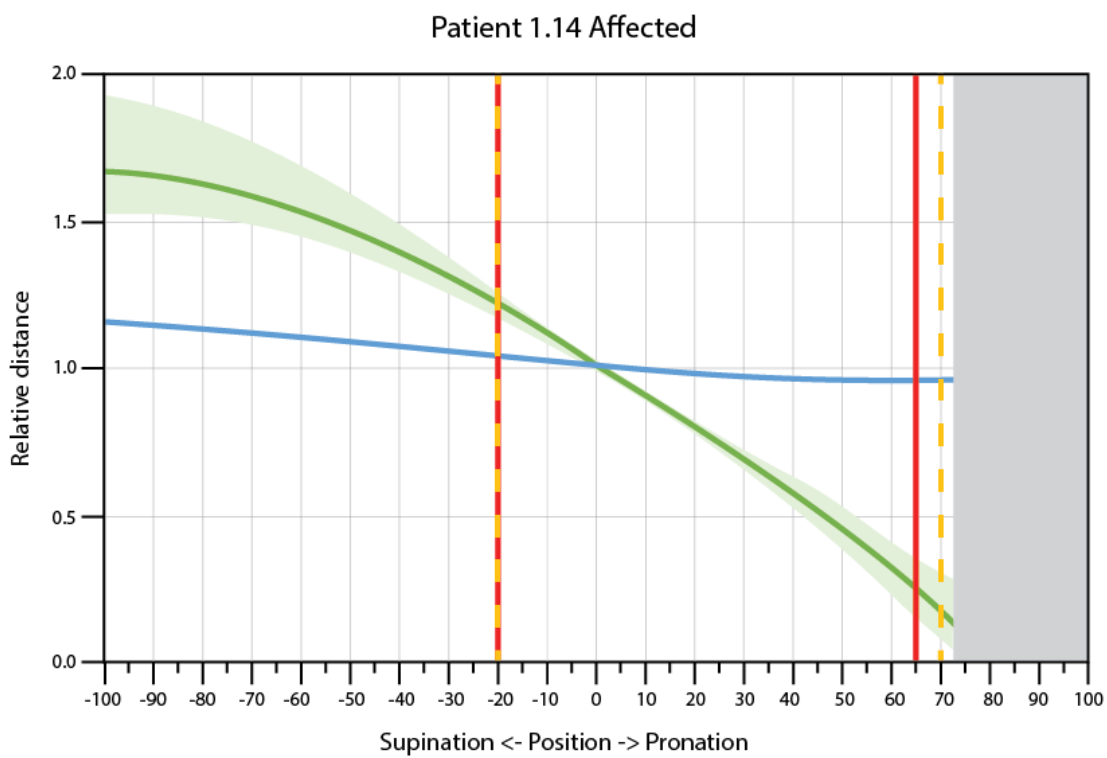


Figure C.29: Model outcomes for patient 1.14 affected forearm

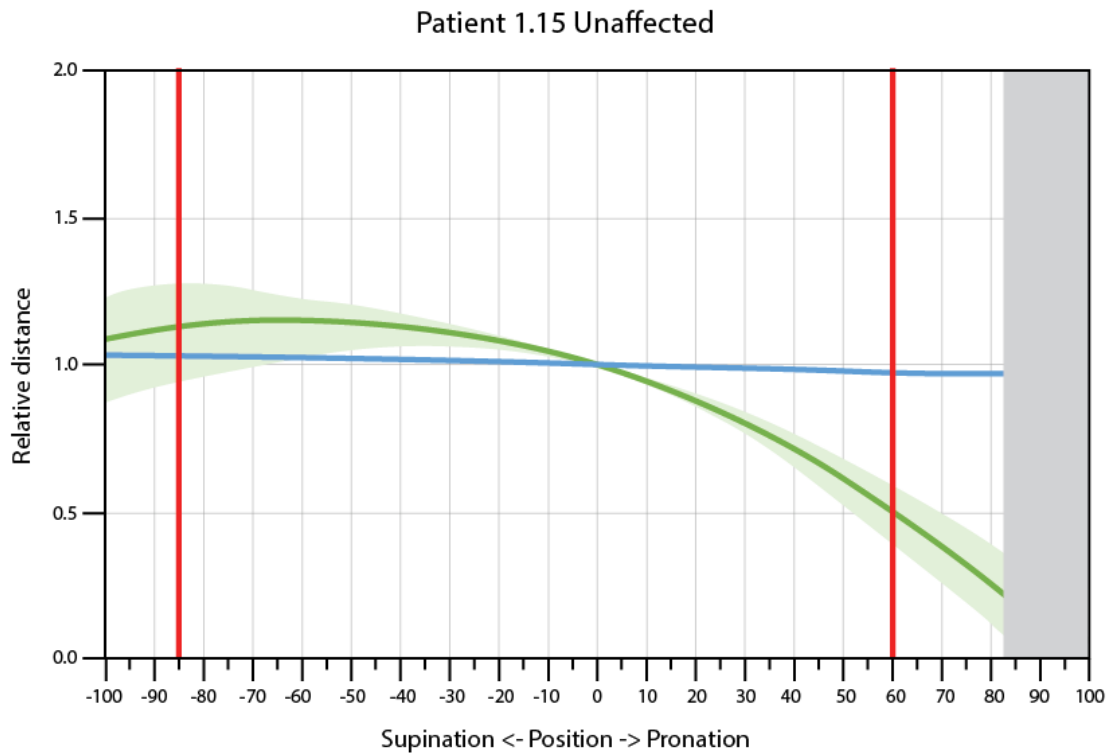


Figure C.30: Model outcomes for patient 1.15 unaffected forearm

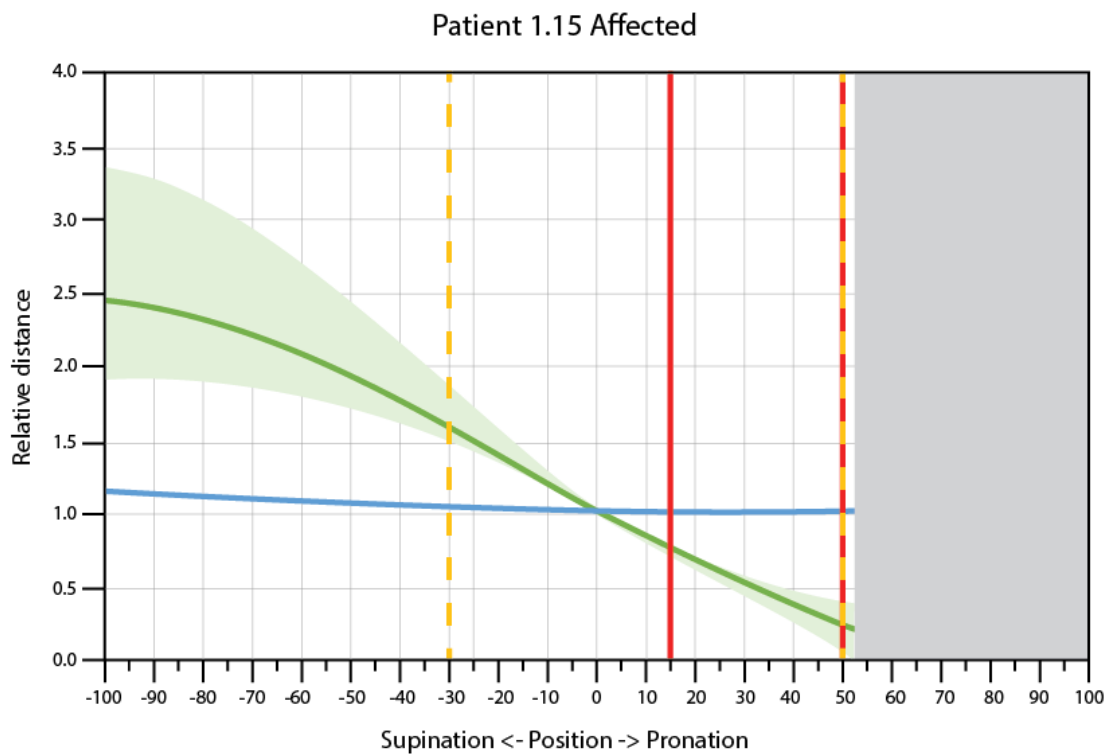


Figure C.31: Model outcomes for patient 1.15 affected forearm

Bibliography

- [1] Shingo Abe et al. “In vivo three-dimensional analysis of malunited forearm diaphyseal fractures with forearm rotational restriction”. In: *JBJS* 100.17 (2018), e113.
- [2] Bardiya Akhbari et al. “Biomechanics of the Distal Radioulnar Joint During In Vivo Forearm Prono-supination”. In: *Journal of Wrist Surgery* (2021).
- [3] Ashley Anderson et al. “Role of the interosseous membrane and annular ligament in stabilizing the proximal radial head”. In: *Journal of shoulder and elbow surgery* 24.12 (2015), pp. 1926–1933.
- [4] Ingrid Andreasson et al. “Functional outcome after corrective osteotomy for malunion of the distal radius: a randomised, controlled, double-blind trial”. In: *International Orthopaedics* 44.7 (2020), pp. 1353–1365.
- [5] Lindsay M Biga et al. “Anatomy & physiology”. In: (2020).
- [6] Florian M Buck et al. “Morphology of the distal radioulnar joint: cadaveric study with MRI and MR arthrography with the forearm in neutral position, pronation, and supination”. In: *American Journal of Roentgenology* 194.2 (2010), W202–W207.
- [7] Andrew E Caputo, Augustus D Mazzocca, and Vincent M Santoro. “The nonarticulating portion of the radial head: anatomic and clinical correlations for internal fixation”. In: *The Journal of hand surgery* 23.6 (1998), pp. 1082–1090.
- [8] DSY Chia, YJ Lim, and WYC Chew. “Corrective osteotomy in forearm fracture malunion improves functional outcome in adults”. In: *Journal of Hand Surgery (European Volume)* 36.2 (2011), pp. 102–106.
- [9] Yoon Seong Choi et al. “Four-dimensional real-time cine images of wrist joint kinematics using dual source CT with minimal time increment scanning”. In: *Yonsei medical journal* 54.4 (2013), pp. 1026–1032.
- [10] John B Christensen et al. “A study of the interosseous distance between the radius and ulna during rotation of the forearm”. In: *The Anatomical Record* 160.2 (1968), pp. 261–271.
- [11] Joost Colaris et al. “Pronation and supination after forearm fractures in children: Reliability of visual estimation and conventional goniometry measurement”. In: *Injury* 41.6 (2010), pp. 643–646.
- [12] Joost Colaris et al. “Angular malalignment as cause of limitation of forearm rotation: an analysis of prospectively collected data of both-bone forearm fractures in children”. In: *Injury* 45.6 (2014), pp. 955–959.
- [13] Jimmy S Daruwalla. “A study of radioulnar movements following fractures of the forearm in children”. In: *Clinical Orthopaedics and Related Research* 139 (1979), pp. 114–120.
- [14] Dawson-Haggerty et al. *trimesh*. Version 3.2.0. URL: <https://trimsh.org/>.
- [15] CE Dumont, R Thalmann, and JC Macy. “The effect of rotational malunion of the radius and the ulna on supination and pronation: AN EXPERIMENTAL INVESTIGATION”. In: *The Journal of bone and joint surgery. British volume* 84.7 (2002), pp. 1070–1074.
- [16] DJ Fuller and CJ McCullough. “Malunited fractures of the forearm in children”. In: *The Journal of bone and joint surgery. British volume* 64.3 (1982), pp. 364–367.
- [17] Karol Galik et al. “The effect of the annular ligament on kinematics of the radial head”. In: *The Journal of hand surgery* 32.8 (2007), pp. 1218–1224.
- [18] Deanna H Gates et al. “Range of motion requirements for upper-limb activities of daily living”. In: *American Journal of Occupational Therapy* 70.1 (2016), pp. 1–10.
- [19] John J Hermans et al. “Anatomy of the distal tibiofibular syndesmosis in adults: a pictorial essay with a multimodality approach”. In: *Journal of anatomy* 217.6 (2010), pp. 633–645.
- [20] Jerry I Huang and Douglas P Hanel. “Anatomy and biomechanics of the distal radioulnar joint”. In: *Hand Clin* 28.2 (2012), pp. 157–63.

- [21] IBM Corp. *IBM SPSS Statistics for Windows*. Version 26.0. Armonk, NY: IBM Corp, 2017. URL: <https://hadoop.apache.org>.
- [22] Sorin Daniel Iordache et al. "Radiation exposure from computed tomography of the upper limbs". In: *Acta Orthop Belg* 83.4 (2017), pp. 581–588.
- [23] Kerwyn Jones and Dennis S Weiner. "The management of forearm fractures in children: a plea for conservatism". In: *Journal of Pediatric Orthopaedics* 19.6 (1999), p. 811.
- [24] Philip Kasten et al. "How does torsional deformity of the radial shaft influence the rotation of the forearm?: a biomechanical study". In: *Journal of orthopaedic trauma* 17.1 (2003), pp. 57–60.
- [25] Brian Katt et al. "Distal radius malunion". In: *The Journal of hand surgery* 45.5 (2020), pp. 433–442.
- [26] Erica Kholinne et al. "The forearm interosseous ligament: comparative mechanical properties of the proximal, central, and distal bands". In: *Journal of Hand Surgery (European Volume)* 46.2 (2021), pp. 184–187.
- [27] Erica Kholinne et al. "The role of the interosseous ligament in forearm rotation: A bio-mechanical study". In: *Journal of Orthopaedic Surgery* 28.3 (2020), p. 2309499020973481.
- [28] Takashi Kitamura et al. "The biomechanical effect of the distal interosseous membrane on distal radioulnar joint stability: a preliminary anatomic study". In: *The Journal of hand surgery* 36.10 (2011), pp. 1626–1630.
- [29] William B Kleinman. "Stability of the distal radioulna joint: biomechanics, pathophysiology, physical diagnosis, and restoration of function what we have learned in 25 years". In: *Journal of Hand Surgery* 32.7 (2007), pp. 1086–1106.
- [30] Theodore T Manson et al. "Forearm rotation alters interosseous ligament strain distribution". In: *The Journal of hand surgery* 25.6 (2000), pp. 1058–1063.
- [31] *Materialise Mimics*. URL: <https://www.materialise.com/en/medical/mimics-innovation-suite/mimics>.
- [32] Joseph C McGinley et al. "MRI detection of forearm soft tissue injuries with radial head fractures". In: *Hand* 9.1 (2014), pp. 87–92.
- [33] J Miyake et al. "Comparison of three dimensional and radiographic measurements in the analysis of distal radius malunion". In: *Journal of Hand Surgery (European Volume)* 38.2 (2013), pp. 133–143.
- [34] Junichi Miyake et al. "3-dimensional deformity analysis of malunited forearm diaphyseal fractures". In: *The Journal of hand surgery* 38.7 (2013), pp. 1356–1365.
- [35] Douglas C Moore et al. "Three-dimensional in vivo kinematics of the distal radioulnar joint in malunited distal radius fractures". In: *The Journal of hand surgery* 27.2 (2002), pp. 233–242.
- [36] Hisao Moritomo et al. "Interosseous membrane of the forearm: length change of ligaments during forearm rotation". In: *The Journal of hand surgery* 34.4 (2009), pp. 685–691.
- [37] Bernard F Morrey. *The elbow and its disorders*. 4th ed. Elsevier Health Sciences, 2009. ISBN: 9781416029021.
- [38] Joshua P Moss and Donald K Bynum. "Diaphyseal fractures of the radius and ulna in adults". In: *Hand clinics* 23.2 (2007), pp. 143–151.
- [39] Alessandro Muntoni and Paolo Cignoni. *PyMeshLab*. Jan. 2021. DOI: 10.5281/zenodo.4438750.
- [40] Ladislav Nagy, Linas Jankauskas, and Charles E Dumont. "Correction of forearm malunion guided by the preoperative complaint". In: *Clinical orthopaedics and related research* 466.6 (2008), pp. 1419–1428.
- [41] Kazuo Noda et al. "Interosseous membrane of the forearm: an anatomical study of ligament attachment locations". In: *The Journal of hand surgery* 34.3 (2009), pp. 415–422.
- [42] Kunihiro Oka et al. "Three-dimensional corrective osteotomy for malunited fractures of the upper extremity using patient-matched instruments: a prospective, multicenter, open-label, single-arm trial". In: *JBJS* 101.8 (2019), pp. 710–721.
- [43] Barry P Pereira, Ashvin Thambyah, and Taeyong Lee. "Limited forearm motion compensated by thoracohumeral kinematics when performing tasks requiring pronation and supination". In: *Journal of applied biomechanics* 28.2 (2012), pp. 127–138.

- [44] Karl-Josef Prommersberger et al. "Rotational deformity in malunited fractures of the distal radius". In: *The Journal of hand surgery* 29.1 (2004), pp. 110–115.
- [45] David Ring. "Treatment of the neglected distal radius fracture". In: *Clinical Orthopaedics and Related Research* 431 (2005), pp. 85–92.
- [46] JA Roberts. "Angulation of the radius in children's fractures". In: *The Journal of bone and joint surgery. British volume* 68.5 (1986), pp. 751–754.
- [47] Kasper C Roth et al. "Factors determining outcome of corrective osteotomy for malunited paediatric forearm fractures: a systematic review and meta-analysis". In: *Journal of Hand Surgery (European Volume)* 42.8 (2017), pp. 810–816.
- [48] Isidro de Jesus Sanchez-Arce et al. "Lateral differences of the forearm range of motion". In: *Proceedings of the Institution of Mechanical Engineers, Part H: Journal of Engineering in Medicine* 234.5 (2020), pp. 496–506.
- [49] Matthew Sardelli, Robert Z Tashjian, and Bruce A MacWilliams. "Functional elbow range of motion for contemporary tasks". In: *JBJS* 93.5 (2011), pp. 471–477.
- [50] Juha-Jaakko Sinikumpu, Tytti Pokka, and Willy Serlo. "The changing pattern of pediatric both-bone forearm shaft fractures among 86,000 children from 1997 to 2009". In: *European journal of pediatric surgery* 23.04 (2013), pp. 289–296.
- [51] M Soubeyrand et al. "Pronation and supination of the hand: Anatomy and biomechanics". In: *Hand Surgery and Rehabilitation* 36.1 (2017), pp. 2–11.
- [52] RICHARD R Tarr, AI Garfinkel, and Augusto Sarmiento. "The effects of angular and rotational deformities of both bones of the forearm. An in vitro study." In: *The Journal of bone and joint surgery. American volume* 66.1 (1984), pp. 65–70.
- [53] Shian Chao Tay et al. "In-vivo kinematic analysis of forearm rotation using helical axis analysis". In: *Clinical Biomechanics* 25.7 (2010), pp. 655–659.
- [54] Jeremy Truntzer et al. "Forearm diaphyseal fractures in the adolescent population: treatment and management". In: *European Journal of Orthopaedic Surgery & Traumatology* 25.2 (2015), pp. 201–209.
- [55] R Shane Tubbs et al. "The oblique cord of the forearm in man". In: *Clinical Anatomy: The Official Journal of the American Association of Clinical Anatomists and the British Association of Clinical Anatomists* 20.4 (2007), pp. 411–415.
- [56] RS Tubbs et al. "The morphology and function of the quadratus ligament". In: *Folia morphologica* 65.3 (2006), pp. 225–227.
- [57] Martin C Tynan et al. "The effects of ulnar axial malalignment on supination and pronation". In: *JBJS* 82.12 (2000), p. 1726.
- [58] Lindsey C Valone et al. "Functional elbow range of motion in children and adolescents". In: *Journal of Pediatric Orthopaedics* 40.6 (2020), pp. 304–309.
- [59] Guido Van Rossum and Fred L. Drake. *Python 3 Reference Manual*. Scotts Valley, CA: CreateSpace, 2009. ISBN: 1441412697.
- [60] Matthew L Vopat et al. "Treatment of diaphyseal forearm fractures in children". In: *Orthopedic reviews* 6.2 (2014).
- [61] Annelie-Martina Weinberg et al. "Which axial deviation results in limitations of pro-and supination following diaphyseal lower arm fracture in childhood?" In: *European Journal of Trauma* 27.6 (2001), pp. 309–316.
- [62] Matthew R Williams and Matthew Varacallo. "Anatomy, Shoulder and Upper Limb, Proximal Radio-Ulnar Joint". In: (2019).
- [63] Ge Wu et al. "ISB recommendation on definitions of joint coordinate systems of various joints for the reporting of human joint motion—Part II: shoulder, elbow, wrist and hand". In: *Journal of biomechanics* 38.5 (2005), pp. 981–992.
- [64] Takashi Yasutomi et al. "Mechanism of limitation of pronation/supination of the forearm in geometric models of deformities of the forearm bones". In: *Clinical Biomechanics* 17.6 (2002), pp. 456–463.